

https://dspace.org/

Experimental estimation of physical properties of a series of rocks from a deep borehole of the Karoo Basin, South Africa

Mahlatji, Merriam

2021
https://hdl.handle.net/10539/33020

Downloaded from a DSpace repository. https://dspace.org/

EXPERIMENTAL ESTIMATION OF PHYSICAL PROPERTIES OF A SERIES OF ROCKS FROM A DEEP BOREHOLE OF THE KAROO BASIN, SOUTH AFRICA

By

Merriam Mahlatji

Student No: 0113611D



UNIVERSITY OF THE
WITWATERSRAND,
JOHANNESBURG

A dissertation submitted to the School of Geosciences, Faculty of Science, University of the Witwatersrand in fulfilment of the requirement for the degree of Master of Science

Supervisor: Prof. Musa Manzi

April 2021

DECLARATION

I declare that this dissertation is my own, unaided work. It is being submitted for the Degree of Master of Science at the University of the Witwatersrand, Johannesburg. It has not been submitted before for any degree or examination at any other University.



Merriam Mahlatji

16th day of November 2021 at The University of Witwatersrand, Johannesburg, South Africa.

Abstract

The aim of this study is to estimate the physical properties (mainly density and seismic velocities) of the deep borehole cores from the Main Karoo Basin (South Africa). The samples were obtained from all the lithological units intersected by the KL1-65 borehole (~ 2034 m deep). The study also investigates the influence of applied uniaxial stress (up to 120 MPa) and mineralogical content on seismic wave propagation through the Karoo Basin rocks. The studied rock samples include sandstone, siltstone, shale, and tillite. The main objectives were to accurately distinguish the geological contacts, delineate the shale gas-bearing formations, and provide guidelines for future laboratory measurements and planning of reflection seismic surveys in the Karoo Basin.

Thirty-eight samples were measured for density and seismic velocity using different techniques to obtain results that would represent true physical properties of the lithological units. Different techniques were used for density measurements, namely the instantaneous water immersion, wax immersion, and calliper methods using ADAM analytical balance scale with a sensitivity of 0.01 g. For ultrasonic measurements, two techniques were used: the Tektronix TDS 2021 and Proceq Pundit Pl 2000 ultrasonic pulser velocity tester consisting of two pairs of transducers with a centre frequency of 54 KHz. The water displacement and water displacement with wax techniques provided similar density results and the latter was chosen owing of its capability to preserve the sample's integrity. Tektronix ultrasonic technique was more preferable over the Proceq technique for velocity measurements conducted under uniaxial stress.

The average density for shale samples was 2.350 g/cm^3, however the density values decreased with increased amount of carbonaceous materials within the sample. Moreover, the more carbonaceous shale from Collingham Formation measured the lower density values (e.g., 2.113 g/cm^3), whilst carbonaceous shales from the Whitehill and Prince Albert Formation (main focus of this study) produced relatively higher average densities (e.g., 2.411 and 2.445 g/cm^3).

The P-wave velocities of sandstone (4500 – 5600 m/s), shale (2100 – 4800 m/s), and siltstone (1700 – 4700 m/s) exhibited an increase in values as a function of depth. The S-wave velocities (Vs) mimicked the P-wave velocity (Vp) throughout the formations. The estimated Vp/Vs relation for sandstone, shale, and siltstone were linear, however the sandstone appears to be slanting horizontal while the relationship for shale and siltstone were directly

proportional with ratio of approximately 1.52, and 1.73 respectively. The information from the Vp-Vs relationship was used to differentiate and identify several lithological units within the Karoo Basin.

Mineralogical analysis indicates that the sandstone packages comprise quartz with relatively high seismic velocities. Shale samples, on the other hand, are mostly clayey with limited transmission of acoustic waves which result in relatively lower seismic velocity values within the package. Seismic velocities for siltstone fluctuate between clayey materials and sandstone rock types as they are a mixture of both.

The estimated bulk densities and seismic velocities were used to compute synthetic seismograms to investigate the potential source of seismic reflectivity and their associated lithological boundaries. The strong reflections were observed at several lithological contacts including Waterford-Kookfontein, Kookfontein-Skoorsteenberg, Skoorsteenberg-Tierberg Formations, and the carbonaceous rich shale formations with the underlying or overlying rocks. The information from the borehole data and synthetic seismograms were used to constrain the seismic interpretation of the legacy 2D reflection seismic data acquired in the area for exploration purposes. Generally, seismic sections exhibit strong reflections at major lithological boundaries and various fault zones cross-cutting the strata. Delineation of faults, in particular, has significant impact on the future exploration projects in the area. Summarily, these results show the importance of analysing more than one sets of data to provide a realistic geological information of the subsurface. Ultimately, the integrated multi-geoscientific data that were collected were used to generate a geological model to provide a better understanding of the existing geological structures in the Karoo Basin.

Acknowledgements

Foremost, I would like to express my sincere gratitude to my supervisor, Prof. Musa Manzi for the continuous support, advice, and immerse knowledge throughout my studies.

I would also like to thank Dr. Emmanuel Onyebueke for his encouragement, enthusiasm, patience, and stimulating discussions, especially in the last months of my research work. I would also like to thank Mr. Andrew Carpede for his technical support by assisting me with sample preparations (e.g., cutting, polishing, etc.).

I would like to thank staff and management of the Council for Geoscience for assistance with all the data that were used for this research. To Dr Muedi, thank you immensely for assisting anywhere possible and being available and Mr. Nxokwana thank you, for generous time and allowing me to learn from you.

Huge thanks to my daughter, Akanani, for being kind and allowing me time to study. To my beautiful five sisters - thank you for all the support and encouragement especially when I thought I couldn’t carry on. To my mom - thank you for always being there and listening to me, and for your unwavering support throughout. To my partner, thank you for your continuous support and guidance. Lastly, thanks to the rest of my family and friends, your support is greatly appreciated.

Contents

DECLARATION ii
Abstract iii
Acknowledgements v
List of Figures viii
1 INTRODUCTION 1
1.1 Background 1
1.2 Aim and objectives 2
2 GEOLOGY OF THE STUDY AREA 4
2.1 Stratigraphy of the Karoo Basin 5
2.2 Geological setting 6
3 LITERATURE REVIEW: PHYSICAL PROPERTIES AND REFLECTION SEISMIC STUDIES 8
3.1 Bulk density 9
3.2 Seismic velocity 9
3.3 Seismic reflection 10
3.4 Seismic data acquisition 11
3.5 Seismic processing and interpretation 12
3.6 Effect of sample size on seismic velocities 12
3.7 Effect of fractures on seismic velocities 14
3.8 Effect of pressure on seismic velocities 14
3.9 Mineralization 15
4 METHODOLOGY 16
4.1 Core sampling 16
4.2 Seismic velocity measurements 17
4.2.1 Tektronix 17
4.2.2 Proceq Pundit PL 2000 18
4.2.3 Velocity measurements under uniaxial stress 21
4.2.4 Density measurements 23
4.2.5 XRD mineralogy 29
4.2.6 Petrography 29
4.2.7 Synthetic seismograms 29
5 RESULTS 31
5.1 Sample description 31
5.2 Density and ultrasonic methods 32
5.3 Bulk density 37

5.4 P-wave and S-wave seismic velocities 38
5.5 Velocity measurements under uniaxial stress 41
5.6 Seismograms 44
5.7 Legacy seismic reflection data acquisition and processing 48
5.8 XRD and petrography results 50
6 INTERPRETATION AND DISCUSSION 53
6.1 Density vs velocity 53
6.2 Relationship between Vp and Vs 55
6.3 Effect of minerals on seismic velocity 59
6.4 Effect of stress on seismic velocities 60
6.5 Synthetic seismogram and seismic interpretation 61
7 CONCLUSION AND RECOMMENDATION 66
8 REFERENCES 68

List of Figures

Figure 1-1: (a) Geological map of South Africa showing the location of the study area and distribution of the Karoo Basin (modified after Johnson, 2006). Note that the red block and red dot show the location of the area and borehole, respectively. (b) Google map indicating the location of the KL1-65 borehole. (c) Google map X Y location of the seismic line and the KL1-65 borehole..... 3

Figure 2-1 The geological map of the Karoo Basin showing the location of KL1-65 borehole (Wikimedia.org/wiki/File: Geology_of_Karoo_Supergroup.png). Note that the dotted lines show the South African boundaries with other Southern African countries. 4

Figure 2-2: Summary of the stratigraphy of the Karoo Basin showing both the western and eastern part of the Main Karoo Basin (modified after Rubidge, 2005). Stratigraphy intersected by the borehole KL1-65 is shown. 5

Figure 3-1: Illustration of reflection seismic survey showing the position of an impact source, the receiver array and the ray path that travel through a two layered medium (modified after Stein and Wysession, 2003). 10

Figure 3-2: Seismic ray reflected at a boundary and obeying Snell's law. P is the P-wave, Vi and ρi are the velocity and density of the respective layer 1 and 2. θ_1 and θ_2 are the incident and refracted angles, respectively, and Z is the layer acoustic impedance. 11

Figure 3-3: An illustration showing high frequency waves as compared to low frequency wave used for sample analysis. 13

Figure 4-1: Laboratory velocity measurement using Proceq instrument. (a) Picture showing the transducer receiver, cylindrical glass rod, and transducer transmitter setup. (b) Calibration of the Proceq instrument using the cylindrical perspex rod. 18

Figure 4-2: A waveform output from the oscilloscope for a sample SM01 showing the location of the first and second arrivals. 20

Figure 4-3: Signal processing steps for sample. (a) First measurement, (b) the measurement number ALL0007 (8^{th} measurement), and (c) the stacked seismogram result produced using all 30 seismograms. 21

Figure 4-4: Illustration of AMSLER compression system with measurements of velocity using Tektronics system. (a) A picture showing the transmitter, core sample, and receiver placement. (b) a picture showing the direction of applied pressure and position of the rotary wheel, and (c) a picture showing the load cell, pulse generator and oscilloscope. 22

Figure 4-5: Adam Model PGW3502i analytical balance scale with a 200 g mass. 24

Figure 4-6: Labotec oven dryer with all samples dried for 24 hours. 24

Figure 4-7: Obtaining volume of a rock sample using the water displacement method. (a) The initial volume of the water in a beaker, and (b) the final volume of the water after immersion of the rock sample. 25

Figure 4-8: Images of the samples dipped in wax with sample numbers for those that needed application of wax and covering the original labelling on the face of the sample. 26

Figure 4-9: Schematic diagram showing how the centre of the core samples were obtained. (a) Step 1, drawing a straight line on one side of the core, (b) Step 2, obtaining two parallel lines of the same length on both side of the core, and (c) Step 3, obtaining the centre of the core by drawing two lines from each end of the core. 28

Figure 4-10: S Synthetic seismogram of P-wave velocity produced using (a)sampling time of 4 ms and frequency of 70 Hz, and (b) 1 ms and frequency of 30 Hz. Note the end result is a multiple of four traces of the same reflection coefficient series of the KL1-65 borehole. The interfaces with reflection coefficient greater than 6% showed strong reflections. 30

Figure 5-1: Effect of pressure on P-wave velocity for sandstone (SM05 and SM12), shales (SM30,SM40 and SM42). The pressure was exerted at a constant increment in the vertical direction perpendicular to the surface of the rock samples. 44

Figure 5-2: Synthetic seismogram of P-wave (a) and S-wave (b) generated using 40 Hz frequency against the stratigraphy associated with borehole lithology. 47

Figure 5-3: (a) Location of the seismic profile WK06_01 and WK06_02 and borehole KL1-65 (pink circle) on Google map (b) Imported location map from oasis Montaj in relation to the position of KL1-65 borehole (yellow) and seismic sections WK06_01 and WK06_02. 49

Figure 5-4: Thin section petrography of SM05 showing composition dominated by quartz, followed by plagioclase and alteration of plagioclase, then mica and other clay minerals. 50

Figure 5-5: Thin section petrography of SM12 showing composition dominated by quartz, followed by plagioclase and its alteration as well as mica and other clay minerals. 51

Figure 5-6: Thin section petrography of SM30 showing dominant composition of quartz followed closely by plagioclase and handful of smectite as well as other clay-rich mineral including mica. 51

Figure 5-7: Thin section petrography of SM42 showing dominant composition of quartz followed closely by mica with other clay-rich mineral and handful of smectite as well as plagioclase. 52

Figure 5-8: Thin section petrography of SM39 showing dominant composition of quartz followed closely by mica with other clay-rich mineral and handful of smectite as well as plagioclase. 52

Figure 6-1: P-wave velocity measurements of all samples plotted against density with red dots representing the shale sample, yellow representing the siltstone, black representing the sandstone and the blue representing the Dwyka tillites. 55

Figure 6-2: Vp vs Vs plots for sandstone (a), siltstone (b), and shale (c) obtained from borehole KL1-65 showing equation obtained for each lithology using the best line fit. 57

Figure 6-3*:* Relationship between Vp/Vs with regards to depth. 58

Figure 6-4: Poisson ratio against depth for borehole KL1-65. 59

Figure 6-5: Synthetic seismogram generated using 40 Hz Ricker wavelet, together with velocity and density laboratory measurements. Note, the RP1 indicates interface between Waterford-Kookfontein, Kookfontein-Skoorsteenberg, and Skoorsteenberg-Tierberg Formation with interbedded shale deposit; the RP2 and RP3 represent the change in grain size within the shale in the Tierberg Formation; and the RP4 represents intercalated black-rich rich from the Tierberg Formation onwards. 63

Figure 6-6: (a) Time -migrated seismic section WK06_02, the red block indicates the extracted seismic part to correlate with the KL1-65 borehole, (b) the KL1-65 borehole correlated with the seismic section and the synthetic seismogram (c) interpreted seismic section indicating the Beaufort Group, Upper Ecca, Lower Ecca, Dwyka and Table Mountain Group. Note, average layered velocity of 5000 m/s was used to estimate the depth values; the black lines represent the faults. 64

Figure 6-7: (a) Time -migrated seismic section WK06_01, (b) Interpreted seismic section WKO6_01 indicating the Upper Ecca, Lower Ecca, Dwyka and Table Mountain Group. The black lines represent the faults delineated on the seismic line; average layered velocity of 5000 m/s was used to estimate the depth values. 65

List of Tables

Table 4-1: BoreholeKL1-65 with location as well as the stratigraphic units intersected. 16

Table 5-1: List of all samples with the sample number measured per formation. 31

Table 5-2: Bulk density measurements of all samples.SM 14 was cut in halves and each sample was labelled with A and B. 34

Table 5-3: Table showing P-wave and S-wave velocities of the samples. 36

Table 5-4: Summary of bulk density, P-wave velocity and S-wave velocity for sandstone samples of the KL1-65 borehole. 39

Table 5-5: Summary of bulk density, P-wave velocity and S-wave velocity for shale samples of the KL1-65 borehole. 40

Table 5-6: Summary of bulk density, P-wave velocity and S-wave velocity for siltstone samples of the KL1-65 borehole. 41

Table 5-7: Summary of bulk density, P-wave velocity and S-wave velocity for siltstone samples of the KL1-65 borehole. 41

Table 5-8: P-wave velocity results of five samples placed under uniaxial pressure. Next to each sample is its respective sample length, L, and diameter of the sample, D. The highlighted rows show the saturation velocity reached in each sample 42

Table 5-9: Physical properties of KL1-65, where Z is the acoustic impedance, Vp is P-wave velocity and Vs is S-wave velocity and Rc is the reflection coefficient. 46

Table 5-10: Table for acquisition parameters of reconnaissance seismic- reflection traverses including WK06_01 and WK06_02 survey lines. 48

Table 5-11 : XRD results of five samples, two sandstone, one siltstone and two samples 53

List of Abbreviations

Abbreviation	Stand for
SOEKER	Southern Oil Exploration Corporation
BV	Bokkeveld Boundary
CDP	Common depth point
CGS	Council For Geoscience
F	Force
F_D	Dominant Frequency
k	constant factor characteristic of spring
M	mass
m/s	Metre per second
MHz	Mega Hertz
NMO	Normal moveout
P	Pressure
Patm	Atmospheric pressure
PPD	Physical Properties Database
RC	Reflection coefficient
RP	reflections packages
RSA	Republic of South Africa
S/N	Signal to noise
SOEKER	Southern Oil Exploration Corporation
TBM	Table Mountain Basement boundary
TWT	Two-way travel time
V	Volume
V_a	P-wave velocity range
Vp	P-wave velocity
Vs	S-wave velocity
W	Weight of the sample
Wdry weight	Weight of the dry sample
WITS	University of the Witwatersrand
Z	Impedance
λ	Wavelength
ρ	Density
Vp	P-wave velocity
Vs	S-wave velocity
P_{atm}	Atmospheric pressure
ρ	Density
λ	Wavelength
V	Volume
W	Weight of the sample
RSA	Republic of South Africa
PPD	Physical Properties Database
TWT	Two-way travel time
WITS	University of the Witwatersrand

1 INTRODUCTION

1.1 Background

The shortage of power in South Africa has opened opportunities for the country to focus on several science disciplines to find alternative energy resources that can complement the current coal-generated energy. Shale gas is one of the few solutions that have been considered because it emits less than 50 - 60% carbon dioxide as compared to coal. The Main Karoo Basin has long been one of the targeted geological environments for oil and conventional gas exploration. Lately, it is targeted because of its potential to host shale gas within some of its formations.

The Karoo Basin has the most prevalent stratigraphic units in Africa (Figure 1.1) and lies south of the Kalahari Desert (Catuneanu *et al*., 2005; Johnson, 2006). The Karoo Basin covers almost two thirds of the southern African landscape including five of the nine provinces within South Africa, and outcrops into the neighboring countries such as Namibia, Mozambique, Botswana, and Zimbabwe (Catuneanu *et al*., 2005; Johnson, 2006; Chere, 2015).

The formation of the Karoo Basin was controlled by tectonism, which modulated the accommodation of placement of volcanic and sedimentary rocks in the Basin with subduction ranging from flexural event in the south to extensional even in the north (Catuneanu *et al*., 2005; Malumbazo, 2016). Catuneanu *et al*. (2005) reported that this tectonic regime was also controlled by climate change from early cold conditions during the Late Carboniferous to warmer, and eventually hot climates with fluctuating precipitation during the deposition of the Karoo sediments (Catuneanu *et al*., 2005). Moreover, the climatic background resulted in the sedimentary depositions that consist of sandstones, shales, and siltstones formations in the Karoo Basin (Malumbazo, 2016).

The shale lithologies can be observed through many of the formations within the Karoo Basin. The gas-bearings strata, which are Permian in age, normally grey to black in colour, are found within the Collingham Formation and/or Tierberg Formation through the Whitehill Formation to the Prince Albert Formation of the Lower Ecca subgroup of the Karoo Basin. The Whitehill Formation is more carbonaceous and organic-rich and contains the most pyrite compared to the underlying Prince Albert and overlying Tierberg Formation (Chere, 2015).

It is paramount to investigate the contacts of shale gas-bearing formations for planning of future exploration projects (mainly seismics). The contact between Whitehill Formation with either Collingham/Tierberg and Prince Albert may be imaged using reflection seismic method if it exhibits a significant contrast in acoustic impedance (Z), which is a product of seismic velocity (V) and bulk density (ρ). However, optimum seismic imaging is also dependent on the thickness, shape, and depth of the target, as well as the signal-to-noise ratio (S/N) of the data (Manzi *et al*., 2012). Acoustic impedance is a physical property used in the seismic method, whereby the wave energy transmitted into the subsurface are reflected, refracted, and diffracted at the interface between two distinctive layers due to acoustic impedance contrast. The difference in acoustic impedance affects the reflection coefficient, which is described as the amount of energy reflected at the geological boundaries ((Z2 – Z1) / (Z2 + Z1)). In that case, the measurements of densities and seismic velocities of core samples obtained from various lithologies in the Karoo Basin require accurate and precise laboratory set-up and techniques to mimic the in-situ environment. The estimated results would assist in designing future reflection seismic surveys; for example, the velocity model derived from these measurements could be used to constrain seismic processing (velocity analysis, static corrections, migration, and time-to-depth conversion). In addition, the study investigates the effects the density, mineralogy, depth, and uniaxial stress might have on the propagation of seismic waves through the Karoo Basin rocks.

1.2 Aim and objectives

The main aim of this study is to characterize physical properties of rocks in the Karoo Basin and understand how these will affect exploration for shale gas.

The main objectives were to conduct laboratory measurements of density and seismic velocity of samples obtained from deep borehole KL1-65 (Figure 1.1b and c) using three different methods in order to obtain the accurate and most representative measurement for each rock property. These objectives were concerned with various tasks of the study to address the following questions:

I. How does the change in stress affect the seismic velocity of the rock?

II. How does mineral composition affect the seismic velocity?

III. Can the shale gas-bearing formation be directly imaged using surface reflection seismic method?

IV. What is the source of seismic reflectivity at the lithological boundaries?

V. What is the thinnest shale layer that can be resolved by reflection seismic method?

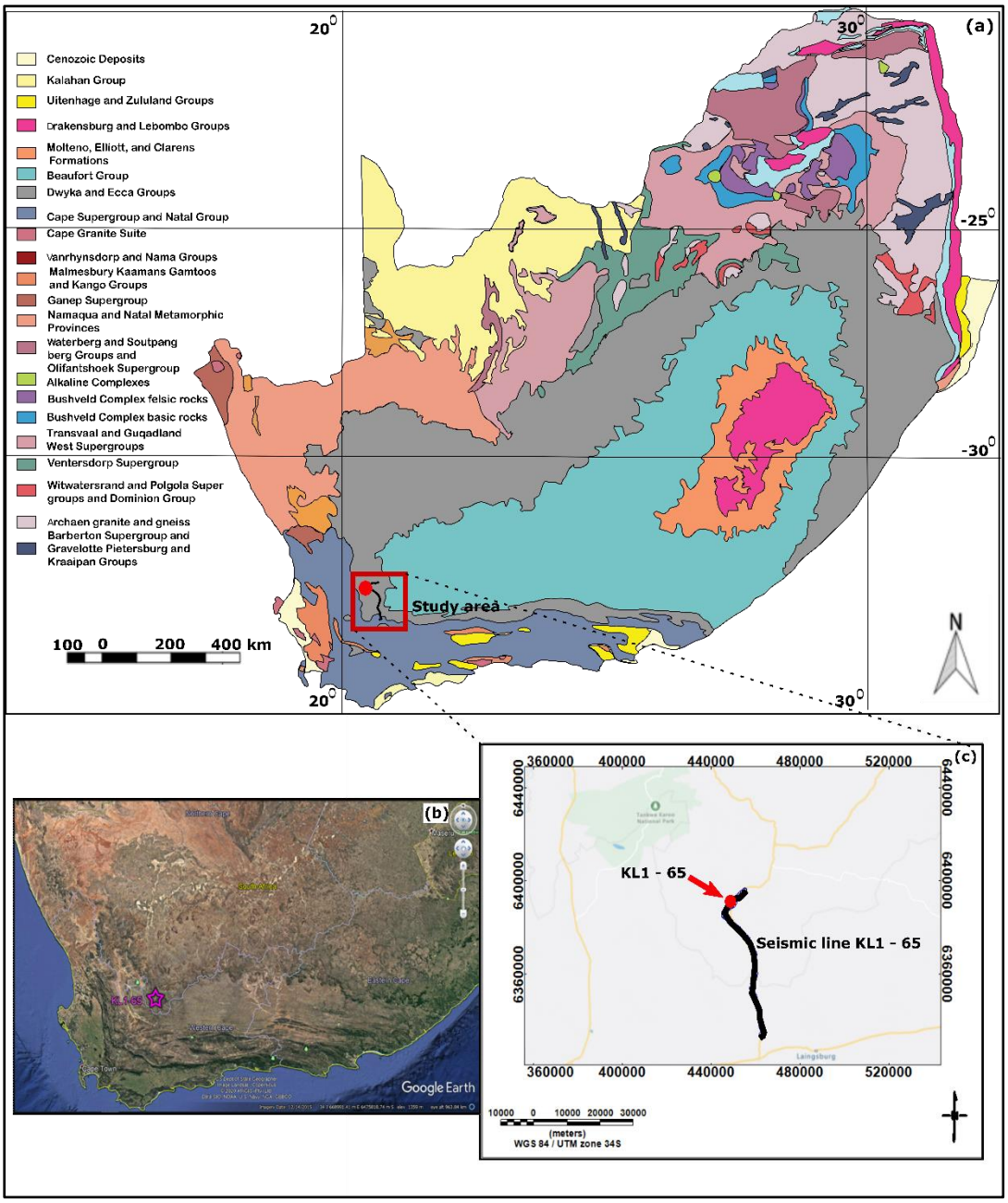


Figure 1-1: (a) Geological map of South Africa showing the location of the study area and distribution of the Karoo Basin (modified after Johnson, 2006). (b) Google earth image indicating the location of the KL1-65 borehole in pink. (c) Google map showing the location of the seismic line (in black) and the KL1-65 borehole (red dot).

2 GEOLOGY OF THE STUDY AREA

The Karoo Supergroup occupies half of South Africa's surface area and extends from the Cape Fold Belt in the south, to the south-eastern boundaries of KwaZulu-Natal and northward into the Northern Cape, Free State and Limpopo provinces (Figure 2.1). The Karoo Basin hosts almost all of South Africa's coal deposits, and it also consists of other resources such as groundwater, coalbed methane, and geothermal energy.

The Karoo Basin has an aerial extent of ~ 550,000 km^2 and has its greatest sedimentary fill along the southern margin of the basin. Sedimentation began in the Carboniferous period with the deposition of the glaciogenic Dwyka Formation (Figure 2.1). The Ecca Group shales were deposited following the retreat of the glacier and the transgression of the Ecca sea (Cadle *et al*., 1993). The carbonaceous shales of the Whitehill Formation of the Ecca Group are being targeted for shale gas potential.

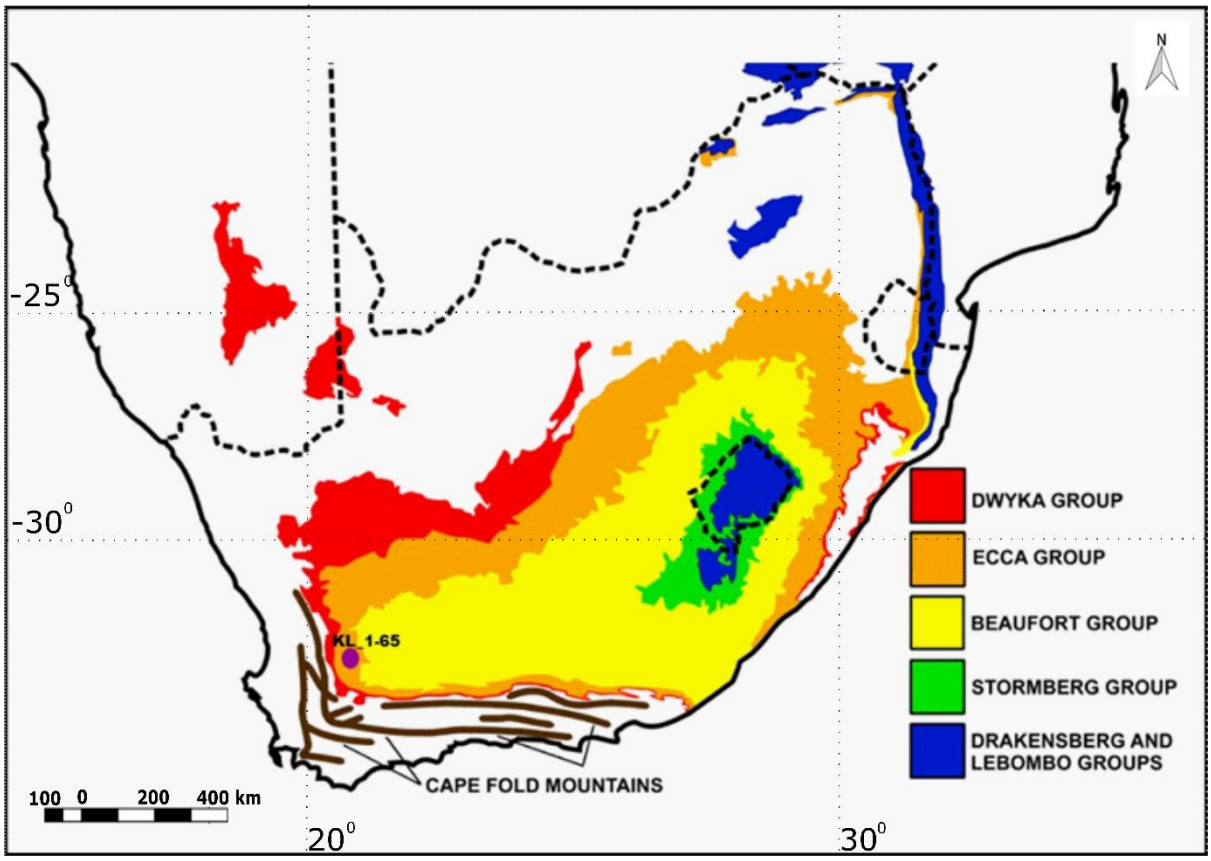


Figure 2-1 The geological map of the Karoo Basin showing the location of KL1-65 borehole (Wikimedia.org/wiki/File: Geology_of_Karoo_Supergroup.png). Note that the dotted lines show the South African boundaries with other Southern African countries.

2.1 Stratigraphy of the Karoo Basin

The stratigraphy of the Karoo Basin is summarised in Figure 2.2, Also shown in Figure 2.2 is the stratigraphy intersected by the borehole KL1-65 located at Klipdrift Farm in Sutherland with coordinates (-32.602, 20.462).

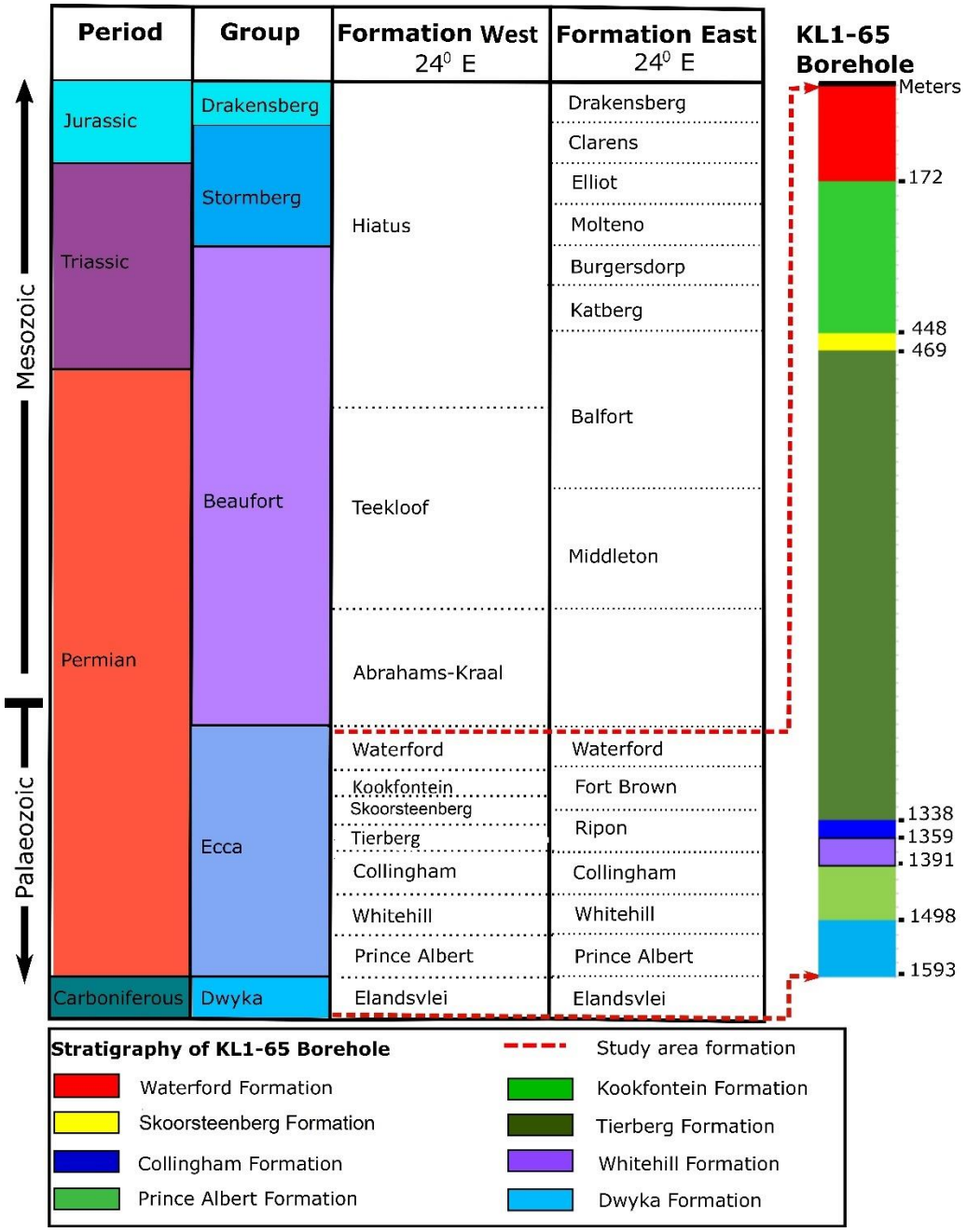


Figure 2-2: Summary of the stratigraphy of the Karoo Basin showing both the western and eastern part of the Main Karoo Basin (modified after Rubidge, 2005). Stratigraphy intersected by the borehole KL1-65 is also shown.

2.2 Geological setting

The Karoo Basin is the most widespread stratigraphic unit in the Kalahari Desert. The sedimentary fill of the Karoo extended from the Late Carboniferous to the Early Jurassic (Smith *et al*, 1993).The strata of the Karoo Basin were deposited in glacial, deep marine (including turbidite), shallow marine, deltaic, fluvial, lacustrine, and Aeolian environments (Johnson, 1996). The Basin is subdivided into several groups, namely the Dwyka, Ecca, Beaufort, Stormberg, Drakensberg and Lebombo Groups (Figure 2.1). The borehole KL1-65 (Figure 2.2) used in this study intersected the following formations from the main groups of the Karoo Supergroup.

- **Dwyka Group**

This is considered to have been deposited in a marine environment (Visser, 1985). It has various types of lithofacies such as massive, carbonaceous, and stratified diamictite, sandstones, and mudrocks. The sandstone facies consist of either very- fine-grained to medium-grained sandstones often interbedded with mudrocks or medium- to - coarse-grained sandstone (von Brunn, 1996). The mudrock facies consist of dark-coloured carbonaceous mudstones, shale, and siltstones.

- **Ecca Group**

This group comprises a total of 16 recognised formations grouped into three geographical area which are the southern, western/ north-western, and north-eastern facies. However, borehole KL1-65 intersected only 7 of these formations.

- **Prince Albert Formation**

The Prince Albert Formation consists mostly of an olive-grey mudrock together with siltstones and shales which are interbedded with the mudstones (Geel, 2015).

- **Whitehill Formation**

The predominant facies are black carbonaceous and pyrite-bearing shales. The shale is very thinly laminated containing high concentration of organic carbon (Geel, 2015). The formation has a thickness between 50 m and 80 m with the maximum observed in western most part of the Karoo Basin (Visser, 1992).

- **Collingham Formation**

This formation comprises of three intercalated lithological units that include fine-grained, poorly sorted, non-fissile mudstone, and very fine grain sandstone. It is predominantly pyroclastic tuffs and fine-grained sandstone (Black, 2015).

- **Tierberg Formation**

The formation comprises well-laminated dark shale, some yellowish tuff and calcareous concretions (Johnson *et al*., 2006).

- **Skoorsteenberg Formation**

This formation comprises five individual sandstone packages (very fine- to – fine grained and light greying), separated by shale units of between 50 – 70 m in thickness (De V. Wickens and Cole, 2017).

- **Kookfontein Formation**

This formation overlies the Skoorsteenberg Formation and coarsens upward. It comprises a sharp contact with predominantly dark grey shale, siltstone and fine- to very fine-grained feldspathic sandstone and averages thickness of 200 m (De V. Wickens and Cole, 2017).

- **Waterford Formation**

Major rock types in this formation are fine-to-medium grained green-grey sandstone, light-brown sandstone, grey mudstone, grey siltstone, and grey-green shale (Geel, 2015).

The three major rock types found in the western part of the Karoo Basin are predominantly sandstone, shale, and siltstone. These three rock types have similar physical properties making it difficult to distinguish each from the other. Therefore, geophysical methods such as reflection seismic and synthetic seismogram modelling are well suited to investigate the different layered sedimentary rock sequences. Consequently, one of the crucial objectives of this project is to determine the smallest shale layer thickness that can be resolved using the seismic reflection method.

3 LITERATURE REVIEW: PHYSICAL PROPERTIES AND REFLECTION SEISMIC STUDIES

This study focuses on characterizing the variations in physical properties along one deep Soekor (Southern Oil Exploration Corporation) borehole drilled within the Karoo Basin. There is a huge academic and public interest to understand the economic potential of shale gas in the Karoo Basin (Cole and Wipplinger, 2001; Cole *et al*, 2011; Kuuskraa and Moodhe, 2013). This study seeks to provide insight by characterizing the geological and geophysical variations along the borehole KL1-65.

The core samples from these boreholes need to be examined for different chemical and physical properties to understand the economic viability of the shale gas resource within the Karoo Basin. For this study, the core samples obtained from the KL65 borehole (~ 1600 m deep), were measured for laboratory physical properties. Different density measurement methods and ultrasonic instruments are used in order to establish the methods that produce accurate results. These measured samples can then be regarded as the best representative samples for the basin.

Understanding physical properties of the rocks is important for future planning of the exploration and resource extraction activities such as seismic surveys and hydraulic fracturing, respectively. For example, understanding the seismic velocities of the rocks may help in constraining numerical simulations to investigate the seismic wave propagation through the solid and fractured rocks. Furthermore, hydraulic fracturing may induce fractures in the rocks depending on the strength of the rocks and alignment of the pre-existing fractures (Liu *et al*, 2018).

Density, P-wave (Vp) and S-wave (Vs) velocities are some of the fundamental physical properties that are important for seismic exploration and drilling. These properties can be measured in respective laboratories using core extracted from implied boreholes. Measurements of these physical properties have long been obtained in the laboratories worldwide. However, very few physical property studies have been conducted for Karoo Basin rocks (Coetzee, 2018). Few factors that influence the physical property measurements include sample size (i.e., diameter; Zhang *et al*., 2002), and length (Karaman *et al*., 2015), pressure or stress (Christensen and Wang, 1985), fractures (Ding *et al*, 2014), mineral alignment (Spagnoli

et al, 2017), and as well as the frequencies of the transducers (transmitters and receivers) used for seismic velocity measurements.

3.1 Bulk density

Archimedes' principle describes the fundamental natural law of buoyancy of any object floating upon or submerged in a fluid. The principle states that an object is buoyed upward by a force equal to the weight of the displaced fluid. This buoyancy is described as the density of a fluid relative to the densities of the submerged objects (Halliday and Resnick, 1988).

Density is denoted as the ratio of the mass of a substance to its volume, expressed in grams per cubic centimeter:

$$\rho = \frac{\text{Weight}}{\text{Volume}}. \quad (1)$$

3.2 Seismic velocity

The seismic velocity is the speed at which an elastic wave propagates through a medium. Body waves that propagate through an elastic material can be compressional waves (also known as P-waves or Vp) or longitudinal waves (also known as shear waves, S-waves or Vs). The velocity of ultrasonic pulses traveling in a solid material depends on the density and elastic properties of that material.

Elasticity is defined as the ability of a body to return to its original shape after removal of distorting stress (Sheriff, 1984). It holds only when the produced strains are infinitesimally small. The term elastic refers to the type of strain that suddenly disappears because of removal of the stress that has caused it. The response of different subsurface media to the wave-induced strains is governed by the elastic constant that regulates the propagation of the seismic wave velocities (Sheriff and Geldert, 1995). The strains due to the passage of seismic waves are quite small and less than of 10^{-8} in magnitude (Sheriff and Geldert, 1995) thereby, confirming the application of Hooke's law in seismic wave propagation from medium to another. Hooke's law is a law of physics that states that the force needed to extend or compress a spring by some distance scales linearly with respect to that distance,

That is,

$$F = kx \qquad (2)$$

Where k is a constant factor characteristic of spring and x is total possible deformation of spring.

The seismic velocity of various sedimentary rocks varies broadly, so it is rather difficult to identify the rock type solely based on a seismic velocity. The velocities, however, are presumed to increase with depth (Schmitt, 2015) but not in all scenarios (e.g., a hidden thin layer of sand channel saddle in between intrusive rocks or stratified sandstone).

3.3 Seismic reflection

Seismic methods involve generating waves that propagate through the subsurface (Lerwill, 1979). The waves are seismic pulses that are generated from a source such as explosion, hammer and vibroseis (Kearey *et al*, 2002) (Figure 3.1**)**.

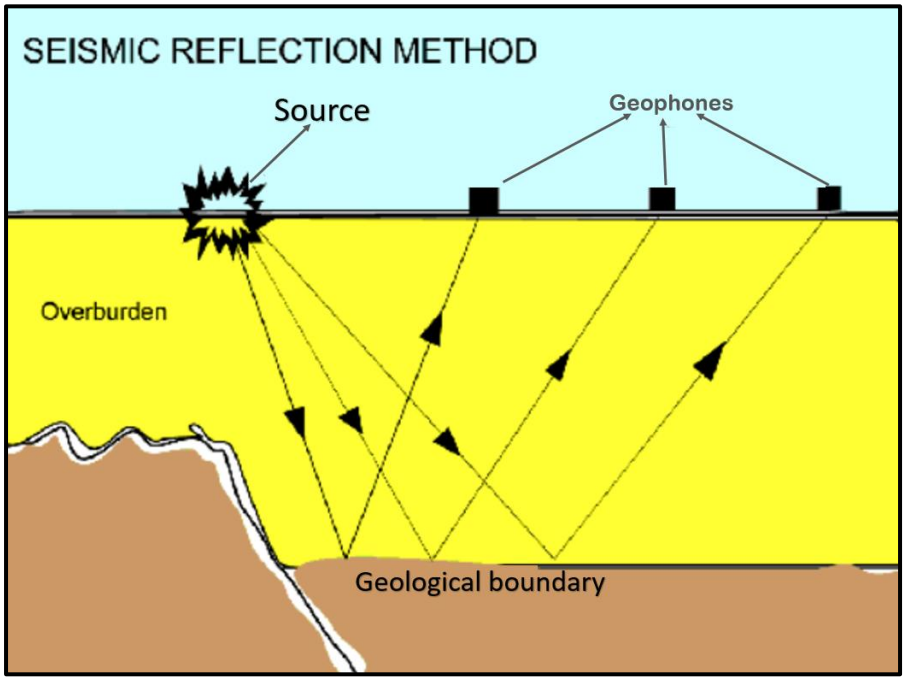


Figure 3-1: Illustration of reflection seismic survey showing the position of an impact source, the receiver array and the ray path that travel through a two layered medium (modified after Stein and Wysession, 2003).

Moreover, the propagation of these seismic waves through layered medium depends on the elastic moduli and density of the rock types that they propagate. The waves are refracted, reflected and/or diffracted at an interface between different rock types (Kearey *et al*, 2002). This scenario is similar to light ray incident at a boundary with high elective index where

Snell's law is observed (Redpath, 1973) (Figure 3.2**)**. Snell's law is a formula used to describe the relationship between incident angle and angle of refraction when light or wave is passed through a boundary between two different media.

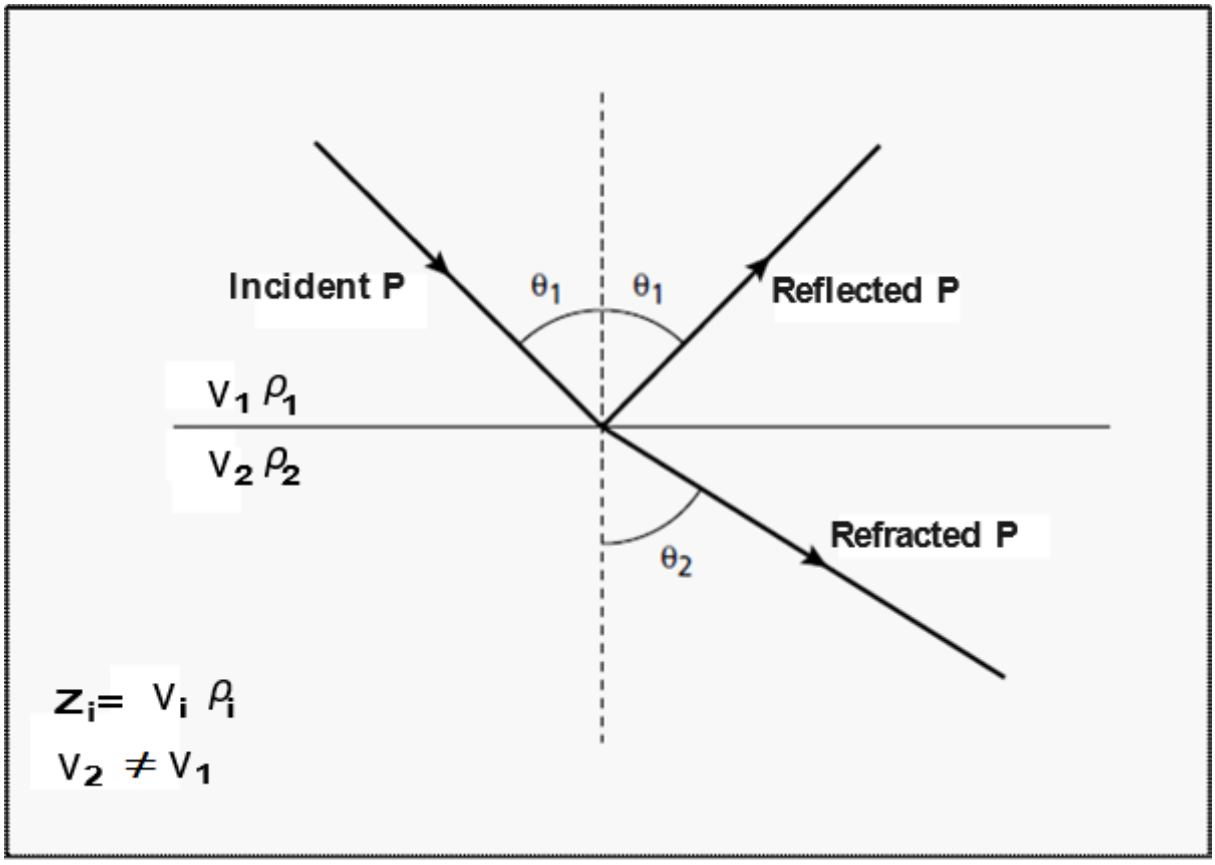


Figure 3-2: Seismic ray reflected at a boundary and obeying Snell's law. P is the P-wave, Vi and ρi are the velocity and density of the respective layer 1 and 2. θ_1 and θ_2 are the incident and refracted angles, respectively, and Z is the layer acoustic impedance.

The seismic waves are then recorded using geophones (Telford *et al*, 1990). The measured time taken to travel through the subsurface at difference ranges from the source may be converted into depth values. These depth values together with the velocity of waves provide reliable information where subsurface geological interfaces may be accurately mapped (Kearey *et al*., 2002).

3.4 Seismic data acquisition

The desired seismic resolution depends on various factors including: source frequency, source spacing, receiver spacing, fold-of-coverage, as well as the depth and shape of the target (Kearey *et al*., 2002). To determine suitable survey parameters, a forward model is conducted using experimental physical property measurements.

Forward modelling is the use of geological and physical property information to produce synthetic seismograms (Krebes, 2004). The seismograms are used to determine if expected geological features will produce reflections at certain lithological contacts (Handwerger *et al*, 2004). They can also be used in aiding other acquisition parameters which will enable better resolutions of the data (Anderson *et al*, 1995). Results from numerical simulations can also be used to understand the physics of the seismic wave propagation and assist in constraining the seismic interpretation.

3.5 Seismic processing and interpretation

Raw seismic data from the field are not ideal for interpretation. In order to create an image that is a representation of subsurface, data must be corrected, and this process is called seismic processing. There are three primary steps needed in processing of seismic data – deconvolution, stacking and migration. Deconvolution compresses the seismic wavelet from the recorded seismic trace to increase resolution. Stacking is a compression process that increases the signal-to-noise ratio of the data. Migration is applied to the stacked or pre-stacked data to collapse diffractions and improve the resolution of the data (Yilmaz, 2001).

After processing, the information obtained from the seismic data is used to infer the geology of the subsurface. There are two basic elements that are recorded in the seismic data that is required by the interpreter, which are time of arrivals and shape of the reflector. From this information conclusions on geological features such as faults and lithological boundaries can be drawn.

3.6 Effect of sample size on seismic velocities

In laboratories, attention to the use of frequency of acoustic source plays an important role. Equipment that uses high frequency sources are preferred to conduct physical property measurements than low frequency sources. The high frequency source produces short wavelengths and guarantee to measure any sample while the low frequency source yield long wavelengths that may completely miss a sample or go through half the sample. The latter will result in misleading results and unreliable conclusions (Figure 3.3).

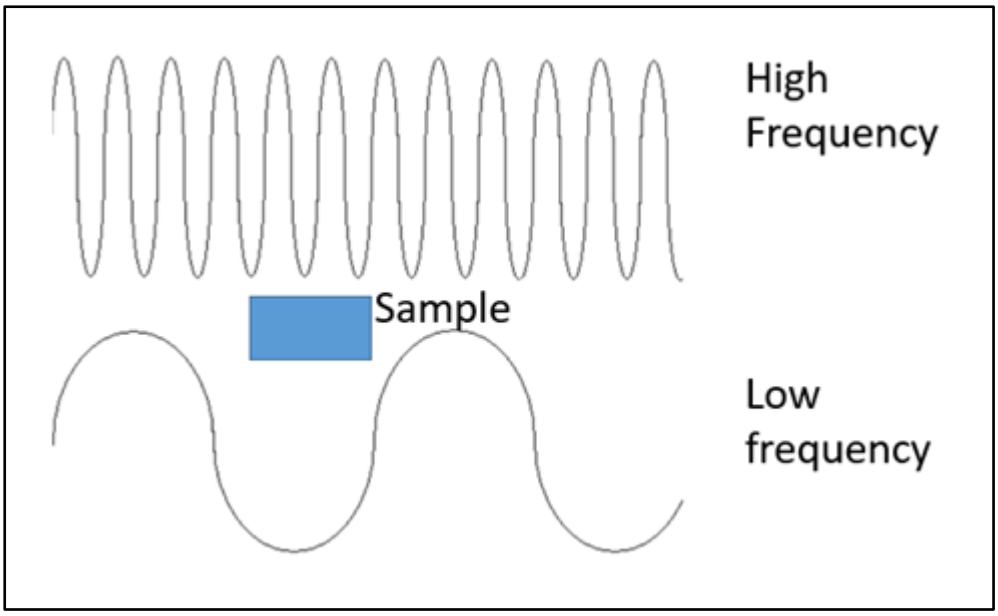


Figure 3-3: An illustration showing high frequency waves as compared to low frequency wave used for sample analysis.

The sample sizes include both the diameters and length of the samples. Few studies have been conducted on how the diameter of rock samples affects the readings (Zhang *et al*., 2002). The authors concentrated particularly on the diameter size of the rock samples. In this study poled and unpoled lead zirconate titanate ceramics were both used to experimentally analyse the extent of influence the sample size has on the ultrasonic measurement. A longitudinal transducer with a center frequency of 15 MHz and diameter of 0.25" together with a Panametric 200 MHz computer-controlled pulser/receiver and a digital oscilloscope Tektronix™ TDS 460A were used to analyse 15 samples. The samples were cut from a large block of ceramic with a height of 5.1 mm. The samples were cut into different lengths and widths ranging from 0.87 mm to 25 mm. They realized that velocity increase is 1.4% and 0.9% in unpoled and poled ceramic samples respectively for the smallest dimension as compared to the bulk values.

Karaman *et al*. (2015) also studied the effect of the specimen length on P-wave velocity in volcanic and limestone rock samples. For their research, Karaman *et al*. (2015) prepared 200 core samples with five different lengths ranging between 50 mm to 150 mm but kept the diameter of 54.7 mm the same for all samples. The ultrasonic pulse method was performed using the Pundit-plus model equipment on dry and saturated samples. The author's evaluations of the test results suggested that the length of the specimen affects the ultrasonic P-wave velocity significantly with fluctuations observed generally in specimens with smaller length.

Fener (2011) also investigated how P-wave velocity is affected by sample dimension using different rock types (e.g., tuff, basalt, limestone, dolomite, granite, ignimbrite, travertine, and andesite) with six different core diameters ranging between 29.68 mm and 113.50 mm. The Pundit 6 Pulse generator unit control and two transducers with frequency of 1 MHz with diameter of 50 mm were used. The test results were statistically analysed using the least squares regression method. A relation between P-wave velocity and sample diameter in tuff and basalt rock group was exponential, while the relation in andesite and ignimbrite rock groups was polynomial. An inverse relationship was observed in limestone, dolomite, tuff, and granite.

3.7 Effect of fractures on seismic velocities

Fractures alter the propagation of the waves through the sample (Boadu and Long, 1996). When fractures are filled with foreign materials the propagation of seismic waves may result in different responses (Berryman, 2007). Hence, it is imperative to understand how the presence of the fractures affect the measurements of elastic properties.

Chen *et al*. (2017) did an experimental study on ultrasonic velocity and anisotropy of deformed coal samples in order to show how the structural fractures can influence the elastic properties of coal samples. The study used 14 samples representative of coal seams and 2 undeformed samples obtained from the mining area east of China and measured using Olympus Model 5077PR Ultrasonic pulser with transducers of 500 KHz. They conclude that the velocity of the deformed samples declined sharply as compared to those that were un-deformed.

Moreover, Ding *et al*. (2014) undertook experimental research using synthetic samples to study the behaviour of Vp and Vs anisotropy in fractured media. They constructed four samples with fractures from synthetic sandstone and they used an ultrasonic experimental system with 0.5 MHz frequency transducers. Ding *et al*. (2014) observed that the measured data were sensitive to fracture density and suggested that the shear wave velocity anisotropy could be a significant characteristic in fractured rock.

3.8 Effect of pressure on seismic velocities

Experimental studies have demonstrated that seismic velocities tend to increase as a function of applied stress or pressure (Nkosi *et al*, 2017). This occurs when the openings of the

existing fractures or pores are forced together to a point where there is no space between them. When the pores or fractures are fully closed then the minerals are in contact creating a closed smooth pathway for the waves to propagate through the sample.

There has always been an interest in the influence of pore pressure on velocities especially in sedimentary rocks. Christensen and Wang (1985) did research to ascertain the influence of the pore pressure and confining pressure on sandstone. For their studies they made use of pulse transmission technique with Lead-zirconate transducers as well as pore pressure and confining pressure hydraulic systems which both use hand pumps. In their findings, they discovered that for an equal increment of increased confining and pore pressure, Vp increased whereas Vs decreased

3.9 Mineralization

Spagnoli *et al*. (2017) measured P-wave and S-wave to differentiate mineralized zones from the host rock. They prepared 40 massive sulphide samples. The measurements were performed using the Panametrics Model 5058P ultrasonic pulser with Agilent DSO 2012A oscilloscope and two 1 KHZ transducers. A coupling fluid was used to ensure that the size of the transducers does not affect the measurements. The resulting seismic velocity results were used to back-calculate porosity, which was correlated with electrical measurements, and both parameters were used to discriminate amongst the sulphide-rich samples.

4 METHODOLOGY

Two different methods (Proceq and Tektronix instruments) were used to conduct ultrasonic measurements (seismic wave velocities) from various samples collected from borehole KL1-65, and three different methods were used for the density measurements.

For density measurements, the measurements were conducted using commonly used techniques in the mining industries: the caliper method, wax immersion method (Crawford, 2013), and instantaneous water immersion method. Due to the soft nature of the samples, some samples were left unsaturated before measurements. However, there were a few samples which were found to be strong enough to go through saturation of over 24 hours.

The samples were obtained from all the lithological units intersected by the KL1-65 borehole. Table 4.1 shows various stratigraphic units intersected by the borehole. The borehole is archived at the national core library of the Council for Geoscience (CGS) at Donkerhoek and was drilled near Sutherland in the Western Cape Province.

Table 4-1: BoreholeKL1-65 with location as well as the stratigraphic units intersected.

Borehole ID	Latitude	Longitude	Name of town	Name of farm	Depth from (m)	Depth to (m)	Stratigraphic unit
KL1/65	-32.602	20.462	Sutherland	KLIP DRIFT 156	0	175.25	Waterford Formation
					175.25	448.34	Kookfontein Formation
					448.34	469.37	Skoorsteenberg Formation
					469.37	1338.92	Tierberg Formation
					1338.92	1359.34	Collingham Formation
					1359.34	1391.95	Whitehill Formation
					1391.95	1498.32	Prince Albert Formation
					1498.32	2034.75	Dwyka

4.1 Core sampling

A total of 41 samples were collected from borehole KL1-65 and marked with their respective sample numbers. The samples were packaged with bubble wrap to avoid breakage.

The samples were removed from the national core library in Donkerhoek, and some were transported to the University of the Witwatersrand, Johannesburg where they were prepared. Samples that couldn't be prepared at the University of the Witwatersrand (WITS) were taken and prepared at the CGS petrophysical laboratory. The core samples were cut flat and polished at each end using cutting machine based at the Rock mechanics laboratory at WITS and the Labotom 5 rock saw machine from CGS. A list of all samples is provided in **Appendix A**.

4.2 Seismic velocity measurements

Seismic method uses the propagation of induced or natural seismic waves through the earth to estimate elastic properties of rock material. The seismic velocity is a function of physical properties of the rock the wave is travelling through. The velocity of a P wave is then expressed as follows:

$$Vp = (B + 1.3G)/\rho)^{1/2}\ , \tag{3}$$

Where ρ is the density of the rock, B is Bulk modulus and G is shear modulus.

The velocity of S-wave is expressed as follows:

$$Vs = (\frac{G}{\rho})^{1/2} \tag{4}$$

Where ρ is the density of the rock, G is the shear modulus. The measurements are expressed in metre per seconds (m/s). For this study, two methods were utilized to measure the seismic velocities of the rock samples.

4.2.1 Tektronix

The seismic velocity measurements were acquired for each sample at room temperature using two pairs of transducers, one operating as the receiver and the other as a transmitter with a centre frequency of 0.5 MHz and diameter of 46 mm. A Panametric 5058 PR was used to generate a pulse and the wave form, the receiving transducer was recorded by a digital oscilloscope (Tektronix TDS 2012 c) connected to the computer. Petroleum-jelly was used as a lubricant for better coupling between the transducers and the sample. The receiver transducer was placed below the sample with the transmitter placed on top of the sample to apply slight

steady pressure in order to produce readings. An aluminium sample with a known velocity was used to calibrate the instruments.

The lengths of all samples were measured using a Vernier caliper with a sensitivity of 0.01 cm, and these measurements were used to calculate the velocity after the picking of the first arrival on the oscilloscope. To reduce the error, each sample was measured 30 times to produce 30 traces; these traces were stacked using SeisRead Matlab code written by Michael Westgate (Coetzee, 2018) to produce one trace with higher S/N.

4.2.2 Proceq Pundit PL 2000

The P- and S- wave velocities were measured on samples at room temperature using Proceq Pundit PL 2000 ultrasonic pulser velocity test instrument with two pairs of transducers with centre frequency of 0.5 MHz. The instrument uses a cylindrical perspex rod as a calibration instrument (Figure 4.1**)**. The length measurements were imported into the system before the sample can be measured. Green sunlight dish washing liquid was used as a coupling between the transducers and the sample. To reduce the error, each sample was measured 30 times and average was calculated.

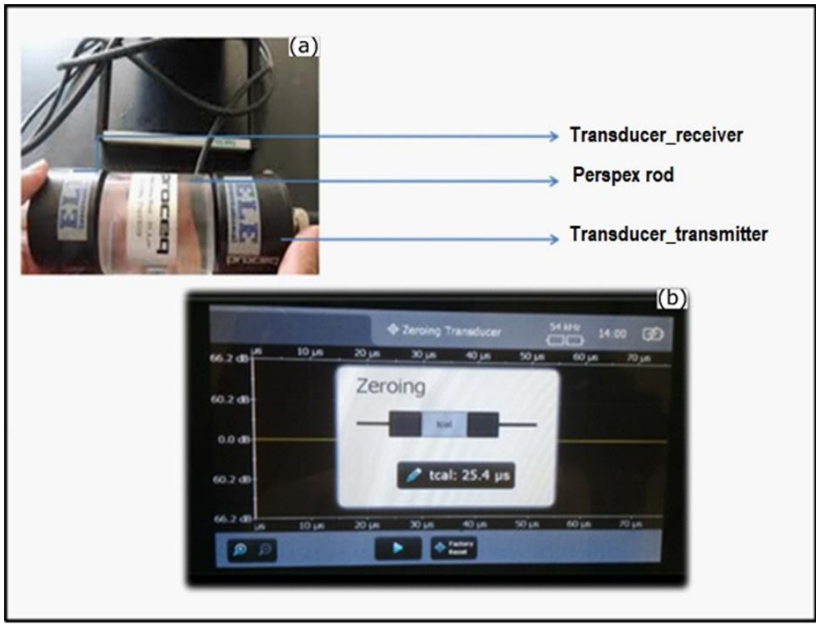


Figure 4-1: Laboratory velocity measurement using Proceq instrument. (a) Picture showing the transducer receiver, cylindrical perspex rod, and transducer transmitter setup. (b) Calibration of the Proceq instrument using the cylindrical perspex rod.

The length measurements were imported into the system before the sample can be measured. Green sunlight dish washing liquid was used as a coupling between the transducers and the sample.

4.2.2.1 Signal processing

Data obtained from Tektronics are then processed to obtain velocity values. Seismic waveform is characterized by the first and second arrival indicating the P-wave and S-wave, respectively (Figure 4.2). Travel time of the P-wave and S-wave are recorded and together with the length of the specimen, P and S-wave velocity are calculated. To eliminate errors, all the 30 measurements obtained from each sample were stacked using a MATLAB based code (written by Michael Westgate, WITS). The most common causes of error are instrumental, human, and random noise produced by vibrations in the laboratory. The code takes all thirty measurements and averages them out to the best fit along the signal's amplitude and with the phase remaining unchanged. Figure 4.3a, b shows the noisy wave forms (or traces) before stacking and Figure 4.3c shows a final stacked data with improved signal-to-noise ratio. It is worth noting that the first arrival is more enhanced on the stacked data as compared to the individual noisy traces.

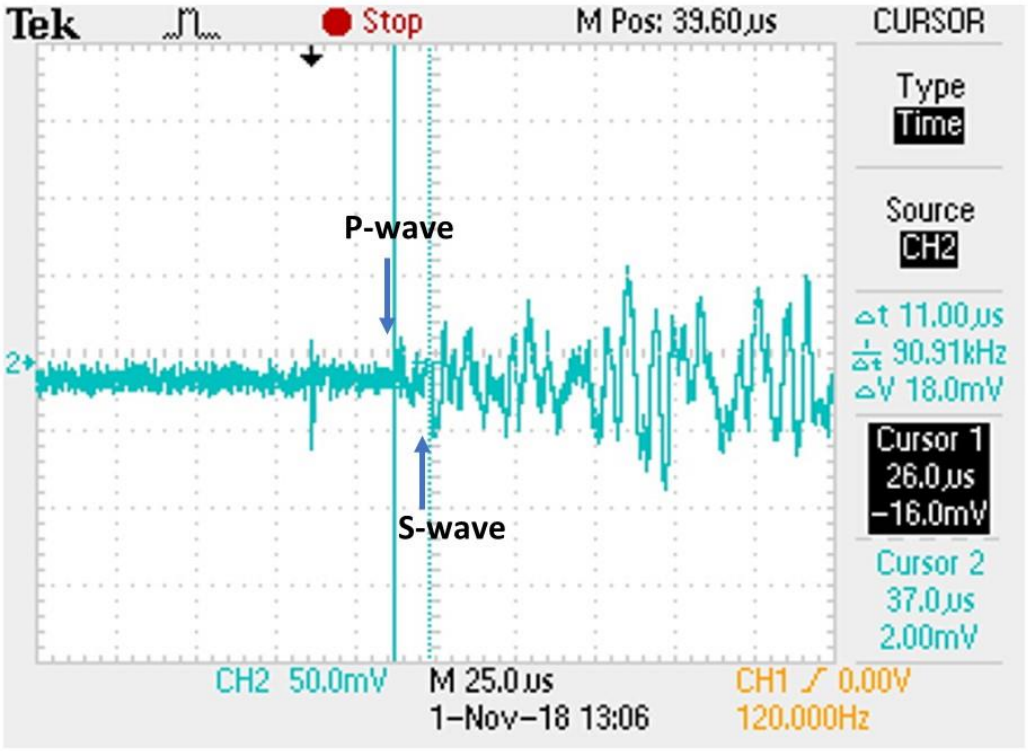


Figure 4-2: A waveform output from the oscilloscope for a sample SM01 showing the location of the first and second arrivals.

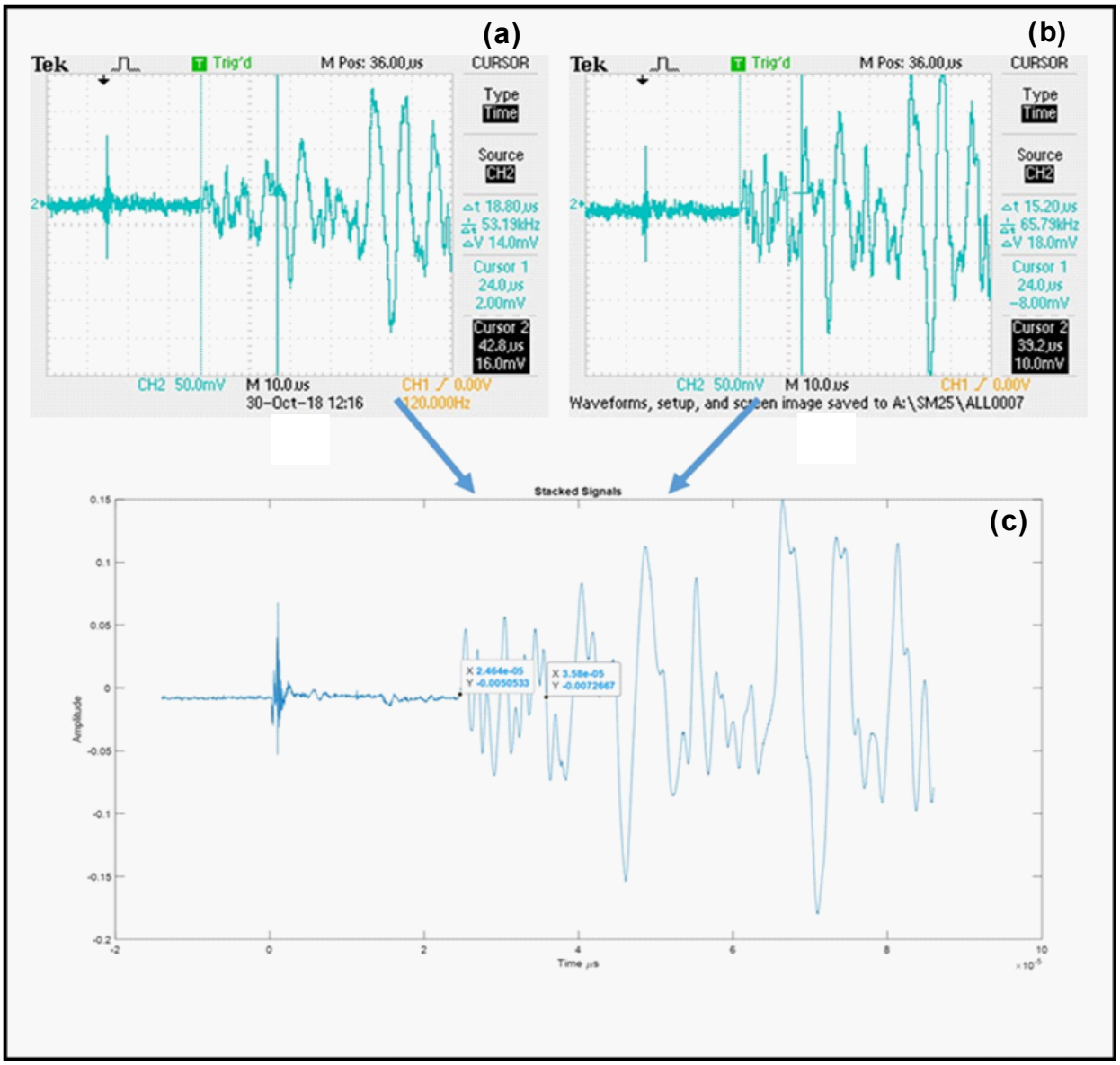


Figure 4-3: Signal processing steps for sample. (a) First measurement, (b) the measurement number ALL0007 (8th measurement), and (c) the stacked seismogram result produced using all 30 seismograms.

4.2.3 Velocity measurements under uniaxial stress

The velocity measurements were acquired using the Tektronics system, but this time under uniaxial stress using the AMSLER compression system (Figure 4.4).

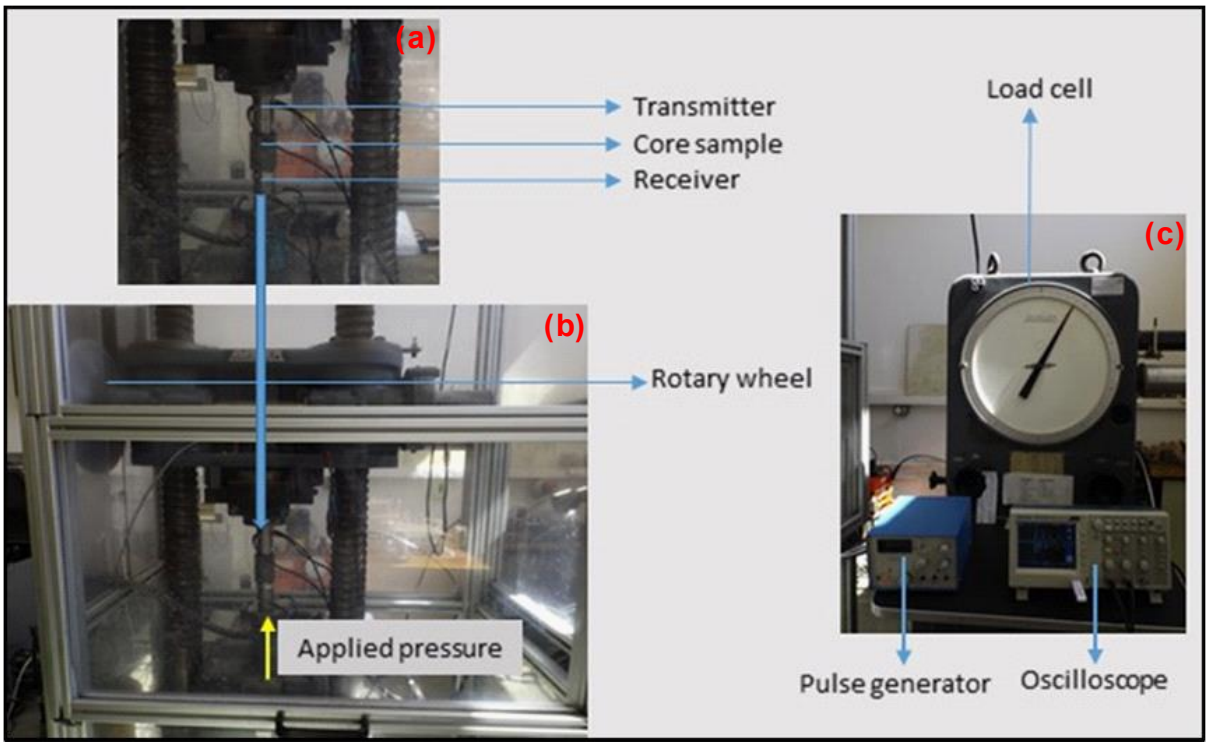


Figure 4-4: Illustration of AMSLER compression system with measurements of velocity using Tektronics system. (a) A picture showing the transmitter, core sample, and receiver placement. (b) a picture showing the direction of applied pressure and position of the rotary wheel, and (c) a picture showing the load cell, pulse generator and oscilloscope.

The AMSLER compression system measures the force exerted on the sample, and pressure is calculated from the measured force using the following equation:

$$P = \frac{F}{A} \qquad (5)$$

where P is Pressure, F is Force exerted on a sample and A is Cross sectional area of a sample.

The Tektronix system was chosen because of the robust nature of the transducers and the ability to lie flat on the surface. The transducers were placed inside the compression system with the loading system acting up from the bottom. The transducers were then connected to the Tektronix system placed outside the compression system for easy acquisition of data (Figure 4.4a).

All seismic velocity measurements were obtained with the loading acting perpendicular to the flat surface of the rock sample with an increment of approximately 6 MPa. The 6 MPa is equivalent to the force of about 20 kN exerted on a core sample with a diameter of 68 mm. The loading of stress was done from 0 kN to 200 kN with an increment of 20 kN 200 kN is close to the maximum overburden stress that can be sustained at a depth of 1.5 km (deepest

position where gas-bearing shale unit can be found within the borehole). If we consider the atmospheric pressure, P_{atm} = 10.1 MPa then the pressure at this depth, P, is

$$P = P_{atm} + g \int_0^z \rho(z)\, dz. \quad (6)$$

The maximum overburden stress at 1.5 km (deepest position where gas-bearing shale unit can be found within the borehole) will be:

$$P = 10.1 \text{ MPa} + (10 * 2.67 * 1.5) \quad (7)$$
$$= 50.1 \text{ MPa} .$$

4.2.4 Density measurements

The density of a rock sample is defined by the ratio of mass to the volume of the rock sample. The measurements obtained are expressed as grams per cubic centimetre (g/cc or g/cm^3). Density measurements were obtained using various methods to compare the methodological results and minimize the errors.

4.2.4.1 Rock mass measurement

The mass of the sample was measured using analytical balance by ADAM Model PGW3502i with sensitivity of 0.01g. The scale is equipped with internally motorised calibration, and a mass piece was used to as a quantitative measure to ensure the correctness of the measurements (Figure 4.5).

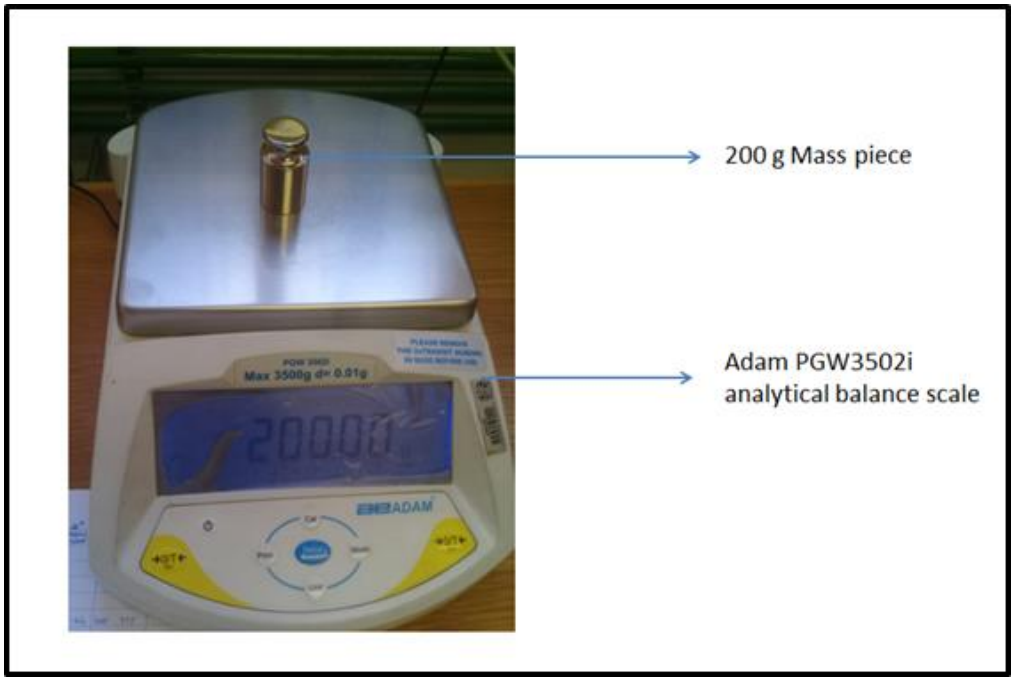


Figure 4-5: Adam Model PGW3502i analytical balance scale with a 200 g mass.

4.2.4.2 Instantaneous water immersion method

For this method a rock sample was firstly dried for 24 hours with a Labotec oven at temperature of 110 degrees Celsius (Figure 4.6**)** and weighed after the sample was cooled down to room temperature for few hours.

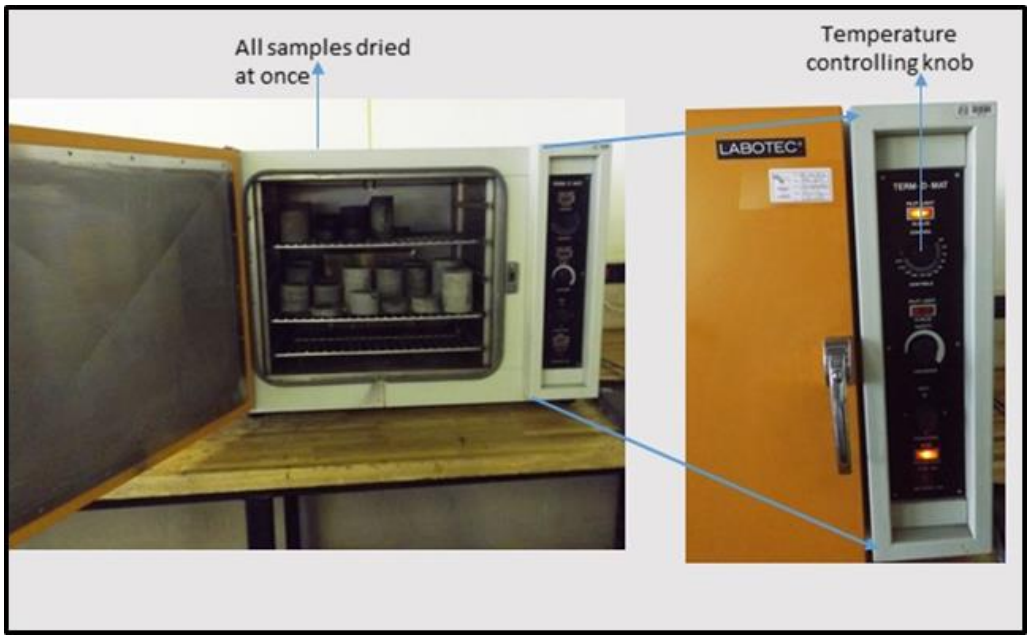


Figure 4-6: Labotec oven dryer with all samples dried for 24 hours.

After weighing, the sample was placed into a volumetric beaker partially filled with distilled water. The sample's volume occupied a certain space within the beaker thereby displacing liquid and raising the water level. The volume of the rock sample was obtained by taking the difference between the two volumes, before and after the rock sample was placed within the volumetric beaker (see equation 6; Figure 4.7).

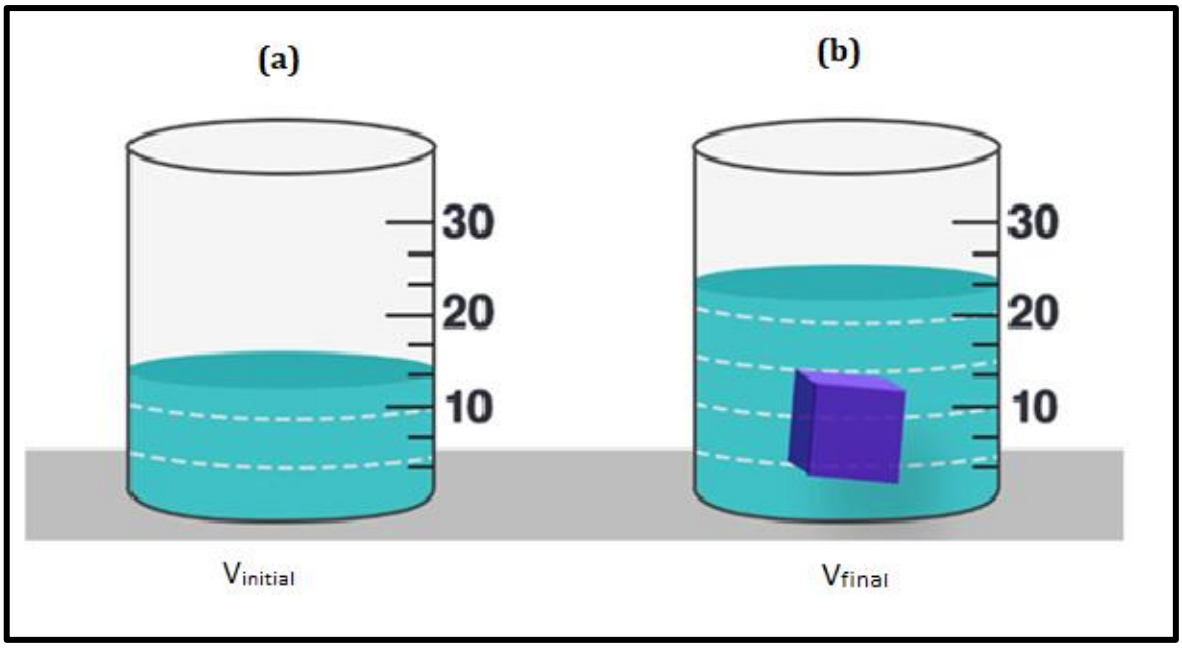


Figure 4-7: Obtaining volume of a rock sample using the water displacement method. (a) The initial volume of the water in a beaker, and (b) the final volume of the water after immersion of the rock sample.

So,

$$V_{sample} = V_{Final} - V_{initial}\,, \qquad (8)$$

Then density (ρ) is calculated as:

$$\rho = \frac{m}{V_{sample}}\,, \qquad (9)$$

Where m is mass of the sample, ρ is density of the sample and V_{sample} is volume of the sample.

4.2.4.3 Wax immersion method

This method is similar to the instantaneous water immersion method; the only difference is that the samples were coated with wax as shown in Figure 4.8. The wax coating is to minimize the impact of water infiltration into the pore spaces. The samples were dried for 24 hours in an oven at temperature of 110 degrees Celsius. The samples were cooled down to room temperature for few hours and then weighed using ADAM analytical balance scale with a sensitivity of 0.01 g. Each sample was then coated with wax by holding one end of the sample and dipping the other end into the wax. The sample was then slowly removed from the wax pan ensuring no bubbles were formed by pressing out the wax on to the sample while it was still warm. The samples were all cooled off and then weighed. Each sample was then placed into the beaker with the known volume, thereby raising the water level. The new volume was measured.

The volume was calculated in two steps. First, the volume of the wax was obtained by subtracting the mass of the sample after overnight dry from the mass of the sample with wax, and this was divided by the density of the wax (~0.87 g/cm^3) (see equations 8 and 9).

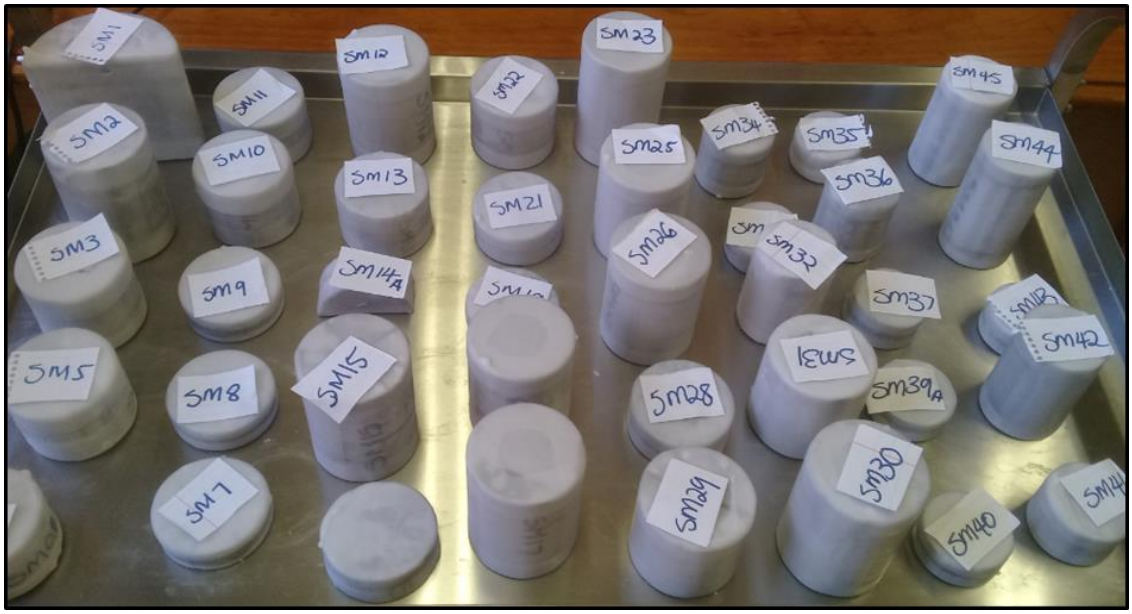


Figure 4-8: Images of the samples dipped in wax with sample numbers for those that needed application of wax and covering the original labelling on the face of the sample.

$$V_{wax} = \frac{W - W_{wax}}{\rho_{wax}}, \qquad (10)$$

where W_{wax} is the weight of the sample coated in wax ,W is the dry weight of the sample, and ρ_{wax} is the density of the wax.

Second step included obtaining the volume of the sample by subtracting the volume of the wax from the volume of the sample with wax, which was the space occupied by the mass within the beaker.

$$V = V_{\text{coated wax}} - V_{\text{wax}}, \quad (11)$$

where V is the volume of the sample without wax coat, $V_{\text{coated wax}}$ is the volume of the sample coated in wax and V_{wax} is the volume of the wax.

So,

$$\rho_{\text{sample}} = \frac{W_{\text{Dry weight}}}{V}, \quad (11)$$

where $W_{\text{dry weight}}$ is the weight of the dry sample, Vis the volume of the sample, and ρ_{sample} is density of the sample.

4.2.4.4 Complete saturation method

This method is similar to the instantaneous water immersion method; the only difference is that the samples were soaked in water at room temperature for 24 hours. The samples were dried for 24 hours in an oven at temperature of 110^0 Celsius. Some samples were not in good conditions and hence this technique was only applied to few samples.

4.2.4.5 Caliper method

This is one of the most basic methods used for determining the bulk density because it requires only a calliper and balance scale. A Vernier caliper with sensitivity of 0.01 mm was used to measure the length and diameter of sample. ADAM Model PGW3502i analytical balance scale with sensitivity of 0.01 g was used to measure the weight of the sample.

However, the method has many limitations, e.g., it requires the sample to be cut into four geometric shapes. For this exercise the samples were not cut for preservation purposes, instead dimensions were drawn out on the face of each sample to measure different diameters.

The diameter was obtained by identifying the centre of the core sample and obtaining two lines of the same length that were drawn parallel to each other on each side of the sample.

Two more chords were drawn from start of one line to the end of the other line, and the position where the two crossing chords met was marked as the centre of the core **(**Figure 4.9**)**.

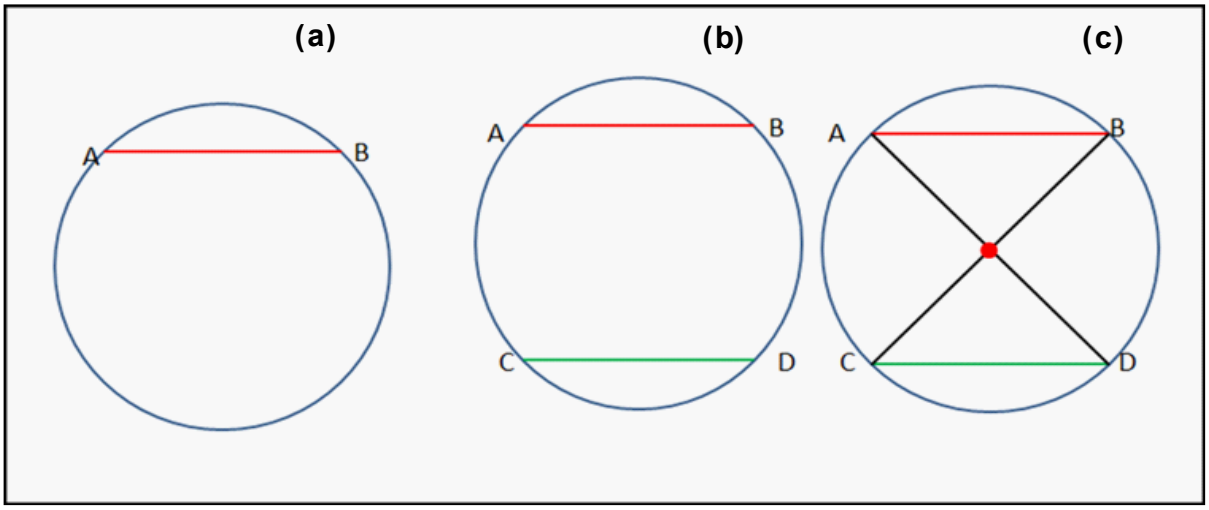


Figure 4-9: Schematic diagram showing how the centre of the core samples were obtained. (a) Step 1, drawing a straight line on one side of the core, (b) Step 2, obtaining two parallel lines of the same length on both side of the core, and (c) Step 3, obtaining the centre of the core by drawing two lines from each end of the core.

The four diameters of the core were obtained using geometry instruments, by drawing a straight line through the centre of the core sample and finding the 45^0 rotations of the core using a compass.

The volume was calculated using the following equation:

$$V = \frac{\pi * L * D}{4}, \qquad (13)$$

where V is the volume of the sample, Lis the length of the sample, and D is the diameter of the sample.

Then the density of the sample was calculated as follows

$$\rho_{sample} = \frac{W}{V}, \qquad (14)$$

where W is the dry weight of the sample, V is the volume of the sample, and ρ_{sample} is the density of the sample.

4.2.5 XRD mineralogy

The samples were prepared, and data were acquired by the Minerology section at Council for Geoscience Laboratory. Prior to sample preparation, the rock sample material was crushed and milled to a fine powder of around 20 μm in size. A sub-sample was pressed into a shallow plastic sample holder against a rough filter paper in order to ensure random orientation. The X-Ray diffraction (XRD) measurements are performed on a BRUKER D8ADVANCE instrument with 2.2 kW Cu long fine focus tube (Cu Kα, λ=1.54060) and 90 position sample changers. The system is equipped with LynxEye detector with 3.7^{Θ} active area where the Θ is the angle between incident ray and the scatter plane when an x-ray is fired onto crystal surface. Samples are scanned from 2^0 to 70^0 2Θ at a speed of 0.02^0 2Θ at a count of 0.5 sec per step, and generator settings of 40 kV and 40 mA.

4.2.6 Petrography

Data for petrography were collected by the Petrography section of the Council for Geoscience Laboratory. A total of 10 thin sections were prepared by cutting the rock sample perpendicular and lateral. The thin sections were investigated under Olympus BX43 microscope with true-colour illumination. An Olympus digital camera connected to both microscope and computer was used to take pictures of the samples.

4.2.7 Synthetic seismograms

The seismograms, Figure 4.10, were generated using SynthSeis Matlab program (Westgate *et al*., 2020). A Ricker wavelet with different frequencies as well as sampling times was used to convolve the reflectivity series obtained from the acoustic impedance calculation. The experimented wavelet frequencies range from 10 to 70 Hz and sampling times were changed from 1 to 4 ms. The different combination frequencies and time sampling play a role on the quality of the seismogram produced. Higher frequencies produced smoother wavelet.

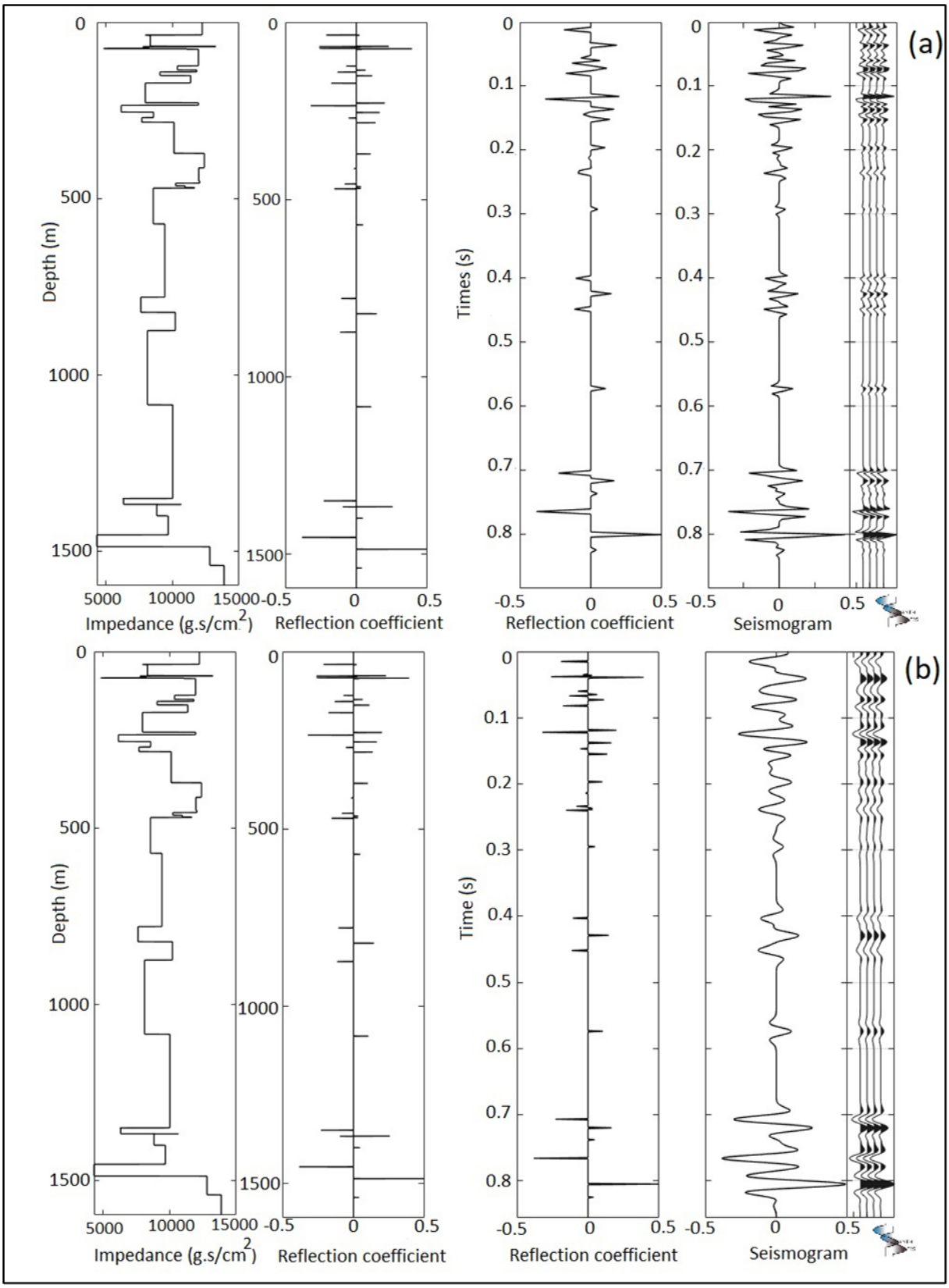


Figure 4-10: S Synthetic seismogram of P-wave velocity produced using (a)sampling time of 4 ms and frequency of 70 Hz, and (b) 1 ms and frequency of 30 Hz. Note the end result is a multiple of four traces of the same reflection coefficient series of the KL1-65 borehole. The interfaces with reflection coefficient greater than 6% showed strong reflections.

5 RESULTS

5.1 Sample description

All 41 samples used in the research are listed in the Appendix A and it is worth noting that these samples are obtained from boreholes which were drilled in the 1960's therefore the measurements obtained are likely to fall on the lower end. Of the total number of samples, 6 are sandstones, 6 are siltstones, 2 are tillites, 1 is a mixture of shale and siltstone, and the rest are shale samples (Table 5.1). The siltstones have different characteristics with some having interbedded layers of shales. The sandstone samples are different with regard to the mineral composition and grain size. Some sandstones are fine-grained while the others are medium-grained sized. There are two types of shale samples. The carbonaceous shales which are blackish in colour and found in the lower Ecca Group (from Collingham to Prince Alberts Formation) and the non-carbonaceous shale samples found at the top part of the stratigraphy.

Table 5-1*:* List of all samples with the sample number measured per formation.

Formation	Shale	Sandstone	Siltstone	Shale/Siltstone	Tilllite
Waterford formation	SM2	SM1	SM6	SM08	
	SM3	SM5	SM7		
	SM9	SM12			
	SM10	SM14A	SM11		
	SM13	SM14B			
	SM15				
Kookfontein Formation	SM16		SM17		
	SM18		SM19		
	SM21		SM22		
	SM23				
Skoortenberg Formation	SM28	SM26			
Tierberg Formation	SM30	SM29			
	SM31				
	SM32				
	SM33				
	SM34				
	SM35				
Collingham Formation	SM36				
	SM37				
Whitehill Formation	SM39				
	SM40				
Prince Albert Formation	SM41				
	SM42				
	SM43				
Dwyka					SM44
					SM45

5.2 Density and ultrasonic methods

The results for bulk densities measured for all the samples are listed in the Table 5.1. The values reported are measurements obtained using the caliper, instantaneous water immersion, wax immersion, and complete saturation, and are rounded to three decimal places. Overall, the instantaneous water immersion and wax immersion methods produced similar values while the caliper results were found to be an over-estimation. For example, the density values for SM11 sample using instantaneous water immersion and wax immersion methods are 2.370 g/cm^3 and 2.232 g/cm^3, respectively. The value for SM11 sample using the Caliper method is 2.628 g/cm^3, which indicates a difference of at least 0.258 g/cm^3.

As much as the wax immersion method was expected to give more accurate results because the wax helps closes off the external pores, the instantaneous method also produced reliable results. For SM33 from the Tierberg Formation measured 2.355 g/cm^3 with the instantaneous water immersion method and 2.283 g/cm^3 with the wax immersion method. The two values fall within the shale density value bracket of 2.250 g/cm^3 and 2.550 g/cm^3 as recorded by the Republic of South Africa Geophysical Rock Properties Database (RSA PPD) situated within the Council for Geoscience (https://www.geoscience.org.za/index.php/2019-03-13-12-40-41/publications/284-geophysical-data). The density and velocity values from formations found within the Karoo Basin are summarised in Appendix, B and C respectively. The caliper method produced a density value of 2.837 g/cm^3.

The wax immersion and caliper methods produced precise values as compared to instantaneous water immersion method. For instance, density values of two sandstone samples (SM25 and SM26) from the Skoorsteenberg Formation measured using the wax immersion method are 2.642 g/cm^3 and 2.645 g/cm^3, respectively. The caliper method, on the other hand, produced values of 2.608 g/cm^3 (SM25) and 2.604 g/cm^3 (SM26), and the instantaneous water immersion produced values of 2.637 gm/cm^3 (SM25) and 2.737 g/cm^3 (SM26).

The wax immersion method was expected to produce more reliable results than other methods for fractured, layered, and porous rock samples because samples were greatly weathered. The sample SM39 A from the Whitehill Formation, shale sample with interbedded layers, measured 2.443 g/cm^3 with the wax immersion method, 2.652 g/cm^3 with caliper method, and 2.433 g/cm^3 with the instantaneous method. The wax immersion value is the

closest to 2.498 g/cm^3, obtained from the lutite (shale) of the Whitehill Formation from RSA PPD, see Appendix B.

Only 5 samples (SM01, SM14 B, SM14 A, SM23, and SM25) were saturated and measured for density measurements. These samples measure relatively higher values than unsaturated samples. For example, SM01 and SM14 B measure 2.692 g/cm^3 and 2.207 g/cm^3, respectively while SM14 A and SM25 measure 2.099 g/cm^3 and 2.636 g/cm^3 respectively. SM23 measures 2.665 g/cm^3, which is closest to the value obtained with wax immersion method (Table 5.2). This method was undertaken particularly to see how complete saturation of samples prior to measurements affect the density of the sample.

Table 5-2: Bulk density measurements of all samples.SM 14 was cut in halves and each sample was labelled with A and B.

Sample ID	Lithology	Stratigraphy	Length (cm)	Caliper (g/cm^3)	Instantaneous Water Immersion (g/cm^3)	Wax Immersion (g/cm^3)	Complete Saturation (g/cm^3)
SM01	Sandstone	Waterford Formation	10.6	*	2.665	2.620	2.692
SM02	Shale		9.71	2.665	2.651	2.630	*
SM03	Shale		6.17	2.651	2.637	2.549	*
SM05	Sandstone		4.95	2.599	2.464	2.358	*
SM06	Siltstone		3.79	2.622	2.411	2.345	*
SM07	Siltstone		1.82	2.625	2.482	2.306	*
SM08	Siltstone/Shale		1.81	2.675	2.339	2.313	*
SM09	Shale		2.33	2.640	2.622	2.601	*
SM10	Shale		5.73	2.659	2.567	2.519	*
SM11	Siltstone		4.82	2.628	2.370	2.233	*
SM12	Sandstone		9.42	2.604	2.594	2.500	*
SM13	Shale		4.85	2.591	2.556	2.524	*
SM14 A	Sandstone		2.92	*	2.030	2.099	2.030
SM14 B	Sandstone		3.16	*	2.037	2.060	2.207
SM15	Shale		9.12	2.656	2.506	2.528	*
SM16	Shale	Kookfontein Formation	2.45	2.555	2.532	2.667	*
SM17	Siltstone		8.82	2.652	2.662	2.485	*
SM18	Shale		8.35	2.648	2.555	2.366	*
SM19	Siltstone		1.23	2.477	2.652	2.645	*
SM21	Shale		3.21	2.639	2.465	2.360	*
SM22	Siltstone		6.08	2.669	2.417	2.373	*
SM23	Shale		10.54	2.871	2.564	2.655	2.665
SM25	Sandstone	Skoorteenberg Formation	8.89	2.608	2.637	2.642	2.636
SM26	Sandstone		8.95	2.604	2.737	2.645	*
SM28	Shale		2.84	2.655	2.509	2.608	*
SM29	Sandstone	Tierberg Formation	6.28	2.627	2.357	2.382	*
SM30	Shale		9.26	2.625	2.608	2.506	*
SM31	Shale		7.08	2.703	2.347	2.305	*
SM32	Shale		7.7	2.739	2.433	2.437	*
SM33	Shale		2.53	2.837	2.355	2.283	*
SM34	Shale		5.08	2.633	2.380	2.282	*
SM35	Shale		2.9	2.673	2.391	2.308	*
SM36	Shale	Collingham Formation	5.78	2.952	2.524	2.503	*
SM37	Shale		3.07	2.508	2.180	2.114	*
SM39 A	Shale	Whitehill Formation	1.97	2.653	2.434	2.442	*
SM40	Shale		2.24	2.761	2.404	2.379	*
SM41	Shale	Prince Albert Formation	3.52	2.661	2.554	2.458	*
SM42	Shale		8.04	2.704	2.435	2.425	*
SM43	Shale		2.47	2.594	2.584	2.453	*
SM44	Tillite	Dwyka	10.34	2.679	2.446	2.508	*
SM45	Tillite		9.15	2.677	2.596	2.559	*

Wax immersion densities are used for seismic analysis in this study because their results proved to be reliable, and in agreement with published results for similar rock types (RSA PPD; Coetzee, 2018). The densities measured by Wax immersion method are reported in table 5.4-5.7 for each lithology.

The results for velocity measured for all the samples are listed in the Table 5.3. The values reported are measurements obtained using Tektronix and Proceq equipment, and the values are rounded to two decimal places. From the 30 ultrasonic measurements recorded for each sample, an average was generated. For Tektronix, wave forms were generated, and the stacking method was used to find an average result. Proceq system generated results in excel format and for that reason a normal mathematical average formula was used. The raw data (data available on disc) from Proceq system results varied quiet largely for other samples. For example, SM02 measured P-wave velocities of 1895 m/s at one point, 2025 m/s next point, and ultimately remained constant at 3880 m/s. The time taken between each measurement was less than a minute. The raw results from the Tektronix system also varied a little; for example, SM02 recorded an initial Vp of 3236 m/s, however an average of 3015 m/s was achieved from stacking 30 traces. The difference between the two systems is that Tektronix's transducers use their own weight to exert pressure to ensure contact with the sample, while Proceq equipment are handheld, and the transducers need applied pressure from the technician to reach contact with the sample. Tektronix applied pressure is constant throughout all samples while for Proceq pressure depends entirely on the technician. Because there was no way of ensuring the same pressure applied for samples Tektronix results are used for this study.

Table 5-3: Table showing P-wave and S-wave velocities of the samples.

Depth	Sample ID	Lithology	Stratigraphy	Length (cm)	Proceq	Tektronix	
					Vp	Vp	Vs
m				cm	m/s	m/s	m/s
36,58	SM1	Sandstone	Waterford Formation	10,60	4906,00	4628,82	3136,09
37,28	SM2	Shale		9,71	3775,00	3015,53	1589,20
68,52	SM3	Shale		6,17	4136,00	3213,54	1301,69
69,52	SM5	Sandstone		4,95	4762,00	5500,00	2079,83
70,56	SM6	Siltstone		3,79	4810,00	3267,24	1592,44
74,46	SM7	Siltstone		1,82	4390,00	3433,96	1400,00
75,56	SM8	Siltstone/Shale		1,81	2400,00	2080,46	896,04
76,84	SM9	Shale		2,33	1643,00	4236,36	2741,18
123,90	SM10	Shale		5,73	1058,00	4696,72	1357,82
135,67	SM11	Siltstone		4,82	5053,00	4504,67	2284,36
141,12	SM12	Sandstone		9,42	4845,00	4640,39	2539,08
151,36	SM13	Shale		4,85	4336,00	3566,18	2819,77
172,58	SM15	Shale		9,12	4789,00	4514,85	2451,61
228,69	SM16	Shale	Kookfontein Formation	2,45	3200,00	3062,50	850,69
235,98	SM17	Siltstone		8,82	2173,00	4642,11	1078,24
255,18	SM18	Shale		8,35	2182,00	2500,00	1035,98
270,75	SM19	Siltstone		1,23	4615,00	3236,84	1757,14
283,86	SM21	Shale		3,21	3200,00	3190,85	1284,00
371,86	SM22	Siltstone		6,08	4803,00	4222,22	2096,55
412,94	SM23	Shale		10,54	5000,00	4747,75	2927,78
450,52	SM25	Sandstone	Skoortenberg Formation	8,89	4918,00	4535,71	2886,36
456,41	SM26	Sandstone		8,95	4891,00	4475,00	2745,40
464,00	SM28	Shale		2,84	4590,00	4000,00	1604,52
468,78	SM29	Sandstone	Tierberg Formation	6,28	5040,00	4617,65	2443,58
470,31	SM30	Shale		9,26	5027,00	4561,58	2684,06
571,90	SM31	Shale		7,08	4057,00	3677,92	1888,00
779,37	SM32	Shale		7,70	4326,00	3869,35	1868,93
822,35	SM33	Shale		2,53	3125,00	3285,71	1664,47
874,20	SM34	Shale		5,08	4854,00	4379,31	2591,84
1084,48	SM35	Shale		2,90	3333,00	3452,38	1686,05
1349,65	SM36	Shale	Collingham Formation	5,78	5273,00	3986,21	2423,48
1351,27	SM37	Shale		3,07	2941,00	2923,81	444,93
1366,48	SM39	Shale	Whitehill Formation	1,97	2532,00	2592,11	956,31
1366,78	SM40	Shale		2,24	6286,00	4462,15	2297,44
1398,76	SM41	Shale	Prince Albert Formation	3,52	2618,00	3520,00	888,89
1452,77	SM42	Shale		8,04	3137,00	3980,20	1240,74
1486,20	SM43	Shale		2,47	2688,00	1715,28	726,47
1539,15	SM44	Tillite	Dwyka	10,34	5074,00	5170,00	2809,78
1593,22	SM45	Tillite		9,15	5750,00	5382,35	2606,84

5.3 Bulk density

SM14 sample was extremely weathered with small pieces falling apart when placed in water during the measurement and was cut into two parts: SM14 A and SM14 B. The average density of this sample was 2.080 g/cm^3, which is less than density of sandstone of 2.680 g/cm^3 as reported by Coetzee (2018). The density measurements of remaining sandstones obtained from the Waterford Formation varied throughout the formation. Most values range between 2.358 g/cm^3 and 2.620 g/cm^3 (Table 5.4). The sandstone density measurements from the Skoorsteenberg Formation varied little throughout the formation. Most values range between 2.642 g/cm^3 and 2.645 g/cm^3 (Table 5.4). The sandstone from the Tierberg Formation has a density value of 2.382 g/cm^3, which is less than all the densities measured from the sandstone rock types. This may imply a general small decrease in seismic velocity with depth (Table 5.4).

The shale density measurements from the Waterford Formation range between 2.524 g/cm^3 and 2.630 g/cm^3 (Table 5.5) and the values show a slight decrease as a function of depth. The Kookfontein Formation shale densities varied throughout the formation ranging between 2.360 g/cm^3 and 2.667 g/cm^3. Only one sample with value 2.608 g/cm^3 from the Skoorsteenberg Formation. The density values from Tierberg Formation varied with a decreasing trend with depth. The values range between 2.282 g/cm^3 (the bottom of the formation) and 2.506 g/cm^3 (top of the formation). Of all the Lower Ecca Group formation samples, the Collingham sample (SM37) has the lowest density of 2.114 g/cm^3 although falls within the published range of between 1.600 g/cm^3 and 2.55 g/cm^3 from the RSA PPD. The other two formations (Whitehill and Prince Albert) exhibit density values with slight variations, ranging between 2.379 g/cm^3 and 2.458 g/cm^3 (Table 5.5). It is, however, worth noting that the Prince Albert shale value is closest to the value of shale obtained from the same formation in the RSA PPD.

The siltstone densities from the Waterford Formation vary little as compared to those from the Kookfontein Formation. The density values from the Waterford Formation range between 2.233 g/cm^3 and 2.345 g/cm^3, while those from Kookfontein Formation range from 2.373 g/cm^3 to 2.645 g/cm^3 (Table 5.6). The tillite density values were measured on two samples and their results vary slightly, e.g., from 2.508 g/cm^3 to 2.559 g/cm^3 (Table 5.7).

5.4 P-wave and S-wave seismic velocities

The P-wave velocity measurements for sandstone varied little in the top section of the stratigraphy with values ranging between 4475 m/s and 5500 m/s (Table 5.4). These values fall within the range published by RSA PPD of 980 m/s – 5500 m/s. Similarly, the S-wave velocities of the sandstone rock varied little with a range between 2079 m/s and 3136 m/s.

The P-wave velocities for shale samples from the top section of the stratigraphy (Waterford – Kookfontein – Skoorsteenberg Formation) varied little (Vp: 3015 m/s and 4747 m/s) except for SM18, which has a P-wave velocity of 2500 m/s (Table 5.5). The results of S-wave velocities, on the other hand, show a noticeable variance with values ranging between 850 m/s and 2927 m/s. The P-wave velocities fall within the P-wave velocity bracket (3545 m/s – 5121 m/s) recorded for shale rock types published by RSA PPD, however the SM16 S-wave velocity value of 850 m/s is visibly low. The shale sample in the Lower Ecca Group exhibits a decrease in Vp as a function of depth, e.g., the lowest Vp value of 1715 m/s was recorded in the Prince Albert Formation. The S-wave velocities from samples within the Lower Ecca Group vary between 444 m/s (recorded within the Collingham Formation) and 2591 m/s (recorded in the Tierberg Formation) (Table 5.5). Overall, P-wave and S-wave velocities show a slight decrease as a function of depth (Table 5.5).

The P-wave velocity values of the siltstone samples from both the Waterford and Kookfontein Formations varied quite considerably, ranging between 2080 m/s and 4642 m/s. The S-wave velocity values for siltstone vary noticeably with values ranging between 896 m/s and 2284 m/s (Table 5.6). The lowest values from both P-wave velocity falls within the bracket of 1710 m/s to 2474 m/s as recorded by RSA PPD.

The tillite P-wave velocity values (i.e., 5170 m/s - 5382 m/s) and S-wave velocities (i.e., 2809 m/s - 2606 m/s) were measured on two samples exhibit little variations (Table 5.7). A few P-wave velocity values are in agreement with records from the RSA PPD with bracket of the P-wave velocities (4500 m/s -5500 m/s).

Table 5-4: Summary of bulk density, P-wave velocity, and S-wave velocity for sandstone samples of the KL1-65 borehole.

Depth (m)	Sample ID	Stratigraphy	Density g/cm^3	Vp m/s	Vs m/s
36,6	SM01	Waterford Formation	2,620	4628,82	3136,09
69,5	SM05		2,358	5500,00	2079,83
141,1	SM12		2,500	4640,39	2539,08
157,0	SM14 A		2,099	*	*
157,0	SM14 B		2,060	*	*
450,5	SM25	Skoorstenberg Formation	2,642	4535,71	2886,36
456,4	SM26		2,645	4475,00	2745,40
468,8	SM29	Tierberg Formation	2,382	4617,65	2443,58

Table 5-5: Summary of bulk density, P-wave velocity, and S-wave velocity for shale samples of the KL1-65 borehole.

Depth (m)	Sample ID	Stratigraphy	Density g/cm^3	Vp m/s	Vs m/s
37,3	SM02	Waterford Formation	2,630	3015,53	1589,20
68,5	SM03		2,549	3213,54	1301,69
76,8	SM09		2,601	4236,36	2741,18
123,9	SM10		2,519	4696,72	1357,82
151,4	SM13		2,524	3566,18	2819,77
172,6	SM15		2,528	4514,85	2451,61
228,7	SM16	Kookfontein Formation	2,667	3062,50	850,69
255,2	SM18		2,366	2500,00	1035,98
283,9	SM21		2,360	3190,85	1284,00
412,9	SM23		2,655	4747,75	2927,78
464,0	SM28	Skoorstenberg Formation	2,608	4000,00	1604,52
470,3	SM30	Tierberg Formation	2,506	4561,58	2684,06
571,9	SM31		2,305	3677,92	1888,00
779,4	SM32		2,437	3869,35	1868,93
822,4	SM33		2,283	3285,71	1664,47
874,2	SM34		2,282	4379,31	2591,84
1084,5	SM35		2,308	3452,38	1686,05
1349,7	SM36	Collingham Formation	2,503	3986,21	2423,48
1351,3	SM37		2,114	2923,81	444,93
1366,5	SM39 A	Whitehill Formation	2,442	2592,11	956,31
1366,8	SM40		2,379	4462,15	2297,44
1398,8	SM41	Prince Albert Formation	2,458	3520,00	888,89
1452,8	SM42		2,425	3980,20	1240,74
1486,2	SM43		2,453	1715,28	726,47

Table 5-6: Summary of bulk density, P-wave velocity, and S-wave velocity for siltstone samples of the KL1-65 borehole.

Depth (m)	Sample ID	Stratigraphy	Density g/cm^3	Vp m/s	Vs m/s
70,6	SM06	Waterford Formation	2,345	3267,24	1592,44
74,5	SM07		2,306	3433,96	1400,00
75,6	SM08		2,313	2080,46	896,04
135,7	SM11		2,233	4504,67	2284,36
236,0	SM17	Kookfontein Formation	2,485	4642,11	1078,24
270,8	SM19		2,645	3236,84	1757,14
371,9	SM22		2,373	4222,22	2096,55

Table 5-7: Summary of bulk density, P-wave velocity, and S-wave velocity for siltstone samples of the KL1-65 borehole.

Depth (m)	Sample ID	Stratigraphy	Density g/cm^3	Vp m/s	Vs m/s
1539,1	SM44	Dwyka	2,508	5170,00	2809,78
1593,2	SM45		2,559	5382,35	2606,84

5.5 Velocity measurements under uniaxial stress

The variation in velocity of rocks under applied uniaxial stress is imperative for the interpretation of seismic data at greater depths. KL1-65 is one of the few boreholes drilled in the Karoo Basin that intersected the Whitehill Formation, which has been targeted for shale gas exploration (Cole *et al*, 2011). To study the effect of stress on seismic velocities, P-wave velocities measurements were conducted under uniaxial stress on five samples from different lithologies. Table 5.8 shows respective values obtained during measurements. The maximum stress of 82 MPa was used for sample with diameter of 68 mm, while a maximum of 129 MPa was used for samples with a small diameter of 54 mm to prevent rock sample from breaking. Three of the samples (SM30, SM40 and SM42) are shales from Lower Ecca Group and two other samples (SM05 and SM12) are sandstones.

Figure 5.1 shows a plot of P-wave velocity as a function of stress (or pressure). All samples exhibit their highest constant P-wave velocities when the maximum stress was reached. Different lithologies exhibit different patterns as a result of the applied uniaxial stress.

For example, the two sandstone samples (SM05 and SM12) exhibit constant P-wave velocities for the first loading stress regime (0-10 MPa), which is followed by a sharp constant increase of approximately 60 m/s with every 10 MPa increment on the loading stress. A saturation stage of P-wave velocity for SM05 (5823 m/s) and SM12 (4095 m/s) was reached at about 43 MPa and 60 MPa, respectively (Table 5.8). For the shale sample, velocity vs stress plot illustrates an increase in P-wave velocity at 0-60 MPa phase For SM40 and SM42. But SM30 showed a slight constant increase in P-wave velocity with the first stress increment (0-60 MPa). A maximum P-wave velocity of 3795 m/s is reached just after 60 MPa for SM30 while SM40 and SM42 reached a higher maximum P-wave velocities of 4785m/s and 5289 m/s, respectively (Table 5.8).

Table 5-8: P-wave velocity results of five samples placed under uniaxial pressure. Next to each sample is its respective sample length, L, and diameter of the sample, D. The highlighted rows show the saturation velocity reached in each sample.

SM30	Tierberg Formation		SM12	Waterford Formation		SM05	Waterford Formation	
Shale	L=94,2mm	D= 68,19mm	Sandstone	L=94,2mm	D= 68,19mm	Sandstone	L=94,2mm	D= 68,19mm
Stress (kN)	P (MPa)	Vp (m/s)	Stress (kN)	P (MPa)	Vp (m/s)	Stress (kN)	P (MPa)	Vp (m/s)
0	0.00	3404.41	0	0.00	3651.16	0	0.00	5500.00
20	5.48	3455.22	20	5.48	3651.16	20	5.48	5500.00
40	10.96	3561.54	40	10.96	3679.69	40	10.96	5500.00
60	16.44	3561.54	60	16.44	3738.10	60	16.44	5561.80
80	21.92	3589.15	80	21.92	3798.39	80	21.92	5625.00
100	27.40	3617.19	100	27.40	3829.27	100	27.40	5689.66
120	32.88	3645.67	120	32.88	3892.56	120	32.88	5755.81
140	38.35	3674.60	140	38.35	3925.00	140	38.35	5755.81
160	43.83	3674.60	160	43.83	3957.98	160	43.83	5823.53
180	49.31	3704.00	180	49.31	3974.68	180	49.31	5823.53
200	54.79	3704.00	200	54.79	4025.64	200	54.79	5823.53
220	60.27	3733.87	220	60.27	4095.65	220	60.27	5823.53
240	65.75	3795.08	240	65.75	4095.65	240	65.75	5823.53
260	71.23	3795.08	260	71.23	4095.65	260	71.23	5823.53
280	76.71	3795.08	280	76.71	4095.65	280	76.71	5823.53
300	82.19	3795.08	300	82.19	4095.65	300	82.19	5823.53

Table 5.8 continuation

SM42	Prince Albert Formation		SM40	Whitehill Formation	
Shale	L=80,4mm	D= 54,4mm	Shale	L=80,4mm	D= 54,4mm
Stress (kN)	P (MPa)	Vp (m/s)	Stress (kN)	P (MPa)	Vp (m/s)
0	0.00	3980.20	0	0.00	3980.20
20	8.61	4102.04	20	8.61	4102.04
40	17.22	4231.58	40	17.22	4231.58
60	25.83	4417.58	60	25.83	4417.58
80	34.44	4466.67	80	34.44	4466.67
100	43.05	4516.85	100	43.05	4516.85
120	51.66	4620.69	120	51.66	4902.44
140	60.26	4785.71	140	60.26	4962.96
160	68.87	4785.71	160	68.87	5025.00
180	77.48	4785.71	180	77.48	5121.02
200	86.09	4785.71	200	86.09	5153.85
220	94.70	4785.71	220	94.70	5153.85
240	103.31	4785.71	240	103.31	5289.47
260	111.92	4785.71	260	111.92	5289.47
280	120.53	4785.71	280	120.53	5289.47
300	129.14	4785.71	300	129.14	5289.47

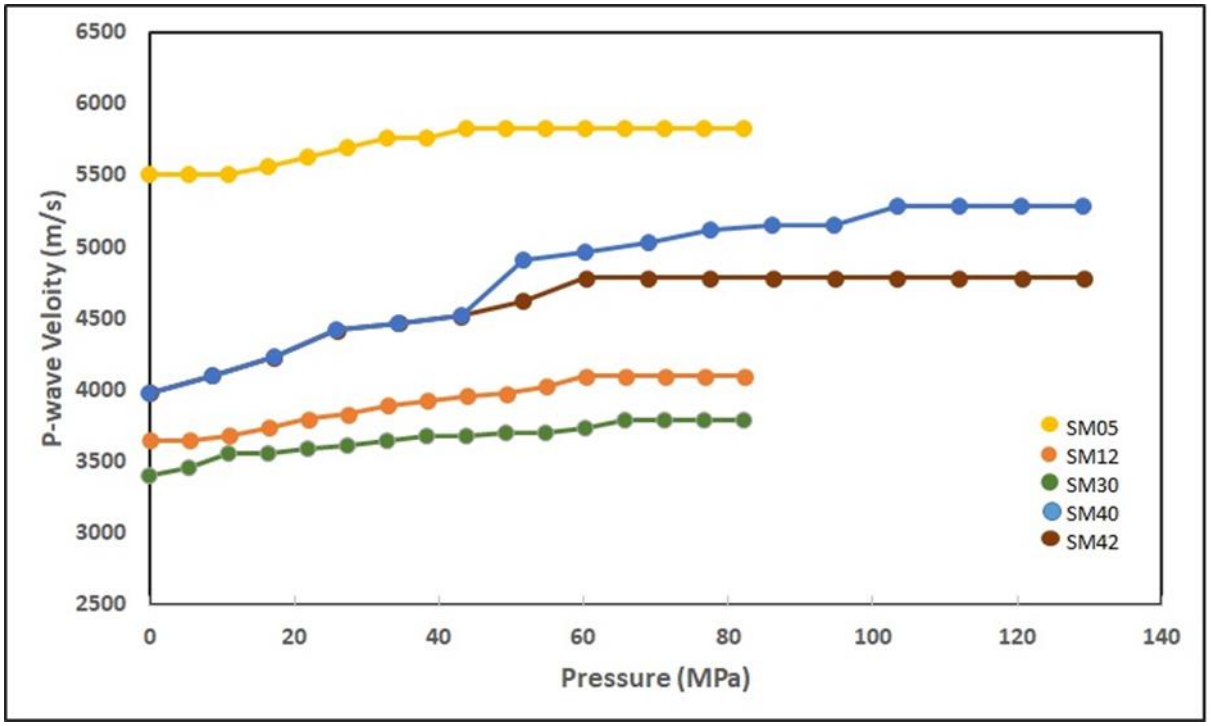


Figure 5-1: Effect of pressure on P-wave velocity for sandstone (SM05 and SM12), shales (SM30, SM40 and SM42). The pressure was exerted at a constant increment in the vertical direction perpendicular to the surface of the rock samples.

5.6 Seismograms

A geological boundary can generate a seismic reflection when there exists a contrast in acoustic impedance between the two boundaries. Reflection coefficient (RC) depends on the acoustic impedance, which is a product of velocity and density. Reflections can be observed when the RC is greater or equal to 0.06 (Sheriff and Gerdart, 1995; Salisbury *et al*, 2003). For example, the RC of 0.025 (Table 5.9) between Kookfontein shale and Skoorsteenberg sandstone interface implies that no strong reflection will be generated at this boundary, implying that it cannot be easily imaged by a surface seismic reflection method. Similar conclusion may be drawn regarding the interface between Skoorsteenberg shale and Tierberg shale with a RC of 0.026 (Table 5.9). However, the interface between Collingham and Whitehill shale resulted in a RC of 0.012, also the RC between Whitehill and Prince Albert shale is 0.102 which suggests that strong reflections will be generated. This implies that a surface reflection seismic method will be successful in mapping the top and bottom of the Whitehill Formation. Similarly, the interface between Dwyka tillite and Prince Albert shale will generate a strong reflection owing to RC of 0.51 (Table 5.9).

To investigate seismic reflectivity along the core sample boundaries, the calculated acoustic impedances and reflection coefficients were used to produce 1D synthetic seismograms (Table 5.9). The synthetic seismograms were generated using SynthSeis program where the reflection coefficient is convolved with Ricker wavelet (zero wavelet). Different frequency values ranging from 10 to 70 Hz were tested. Ultimately the 40 Hz Ricker wavelet was selected to create the synthetic seismogram, Figure 5.2, since the dominant frequency (F_D) of the legacy seismic reflection data is calculated to be 40 Hz. The dominant frequency is calculated by dividing the wavelength from seismic velocity. The wavelength determines the resolution, so in return dominant frequency play a role in determination of vertical resolution since seismic velocity is an independent property that cannot be changed. In essence the only changes that can be applied during processing of data to increase the resolution is that of frequency.

The data show reflection coefficients between different lithologies ranging between 0.016 and 0.51. Evidently, a reflection coefficient of approximately 0.253 was observed when shale was interbedded within other shale units. This phenomenon is observed within the Whitehill Formation where the shale unit becomes more carbonaceous towards the bottom the formation. This also means that the contact within the shale unit separating the more carbonaceous shale unit from the shale unit is mapped.

Table 5-9: Physical properties of KL1-65, where Z is the acoustic impedance, Vp is P-wave velocity and Vs is S-wave velocity and Rc is the reflection coefficient.

Stratigraphy	Depth	Sample	Litholog	Vp	Vs	Density	Z	Rc
	m			m/s	m/s	g/cm^3	g/m^{2}s	
Waterford Formation	36.58	SM1	Sandstone	4628.82	3136.09	2.62	12.128	0.209
	37.28	SM2	Shale	3015.53	1589.2	2.63	7.931	-0.016
	68.52	SM3	Shale	3213.54	1301.69	2.55	8.191	-0.226
	69.52	SM5	Sandstone	5500	2079.83	2.36	12.968	0.257
	70.56	SM6	Siltstone	3267.24	1592.44	2.34	7.661	-0.016
	74.46	SM7	Siltstone	3433.96	1400	2.31	7.917	0.244
	75.56	SM8	Siltstone/Shale	2080.46	896.04	2.31	4.812	-0.392
	76.84	SM9	Shale	4236.36	2741.18	2.6	11.02	-0.035
	123.9	SM10	Shale	4696.72	1357.82	2.52	11.829	0.081
	135.67	SM11	Siltstone	4504.67	2284.36	2.23	10.057	-0.071
	141.12	SM12	Sandstone	4640.39	2539.08	2.5	11.6	0.126
	151.36	SM13	Shale	3566.18	2819.77	2.52	9.002	-0.118
	172.58	SM15	Shale	4514.85	2451.61	2.53	11.414	0.166
Kookfontein Formation	228.69	SM16	Shale	3062.5	850.69	2.67	8.169	-0.171
	235.98	SM17	Siltstone	4642.11	1078.24	2.48	11.534	0.322
	255.18	SM18	Shale	2500	1035.98	2.37	5.914	-0.183
	270.75	SM19	Siltstone	3236.84	1757.14	2.65	8.561	0.064
	283.86	SM21	Shale	3190.85	1284	2.36	7.531	-0.142
	371.86	SM22	Siltstone	4222.22	2096.55	2.37	10.021	-0.114
	412.94	SM23	Shale	4747.75	2927.78	2.66	12.607	0.025
Skoortenberg Formation	450.52	SM25	Sandstone	4535.71	2886.36	2.64	11.985	0.006
	456.41	SM26	Sandstone	4475	2745.4	2.65	11.836	0.063
	464	SM28	Shale	4000	1604.52	2.61	10.434	-0.026
Tierberg Formation	468.78	SM29	Sandstone	4617.65	2443.58	2.38	11	-0.019
	470.31	SM30	Shale	4561.58	2684.06	2.51	11.433	0.148
	571.9	SM31	Shale	3677.92	1888	2.31	8.478	-0.053
	779.37	SM32	Shale	3869.35	1868.93	2.44	9.431	0.114
	822.35	SM33	Shale	3285.71	1664.47	2.28	7.5	-0.143
	874.2	SM34	Shale	4379.31	2591.84	2.28	9.994	0.113
	1084.48	SM35	Shale	3452.38	1686.05	2.31	7.969	-0.112
Collingham Formation	1349.65	SM36	Shale	3986.21	2423.48	2.5	9.979	0.235
	1351.27	SM37	Shale	2923.81	444.93	2.11	6.181	-0.012
Whitehill Formation	1366.48	SM39 A	Shale	2592.11	956.31	2.44	6.331	-0.253
	1366.78	SM40	Shale	4462.15	2297.44	2.38	10.616	0.102
Prince Albert Formation	1398.76	SM41	Shale	3520	888.89	2.46	8.653	-0.055
	1452.77	SM42	Shale	3980.2	1240.74	2.42	9.651	0.393
	1486.2	SM43	Shale	1715.28	726.47	2.45	4.207	-0.51
Dwyka	1539.15	SM44	Tillite	5170	2809.78	2.51	12.965	-0.03
	1593.22	SM45	Tillite	5382.35	2606.84	2.56	13.772	

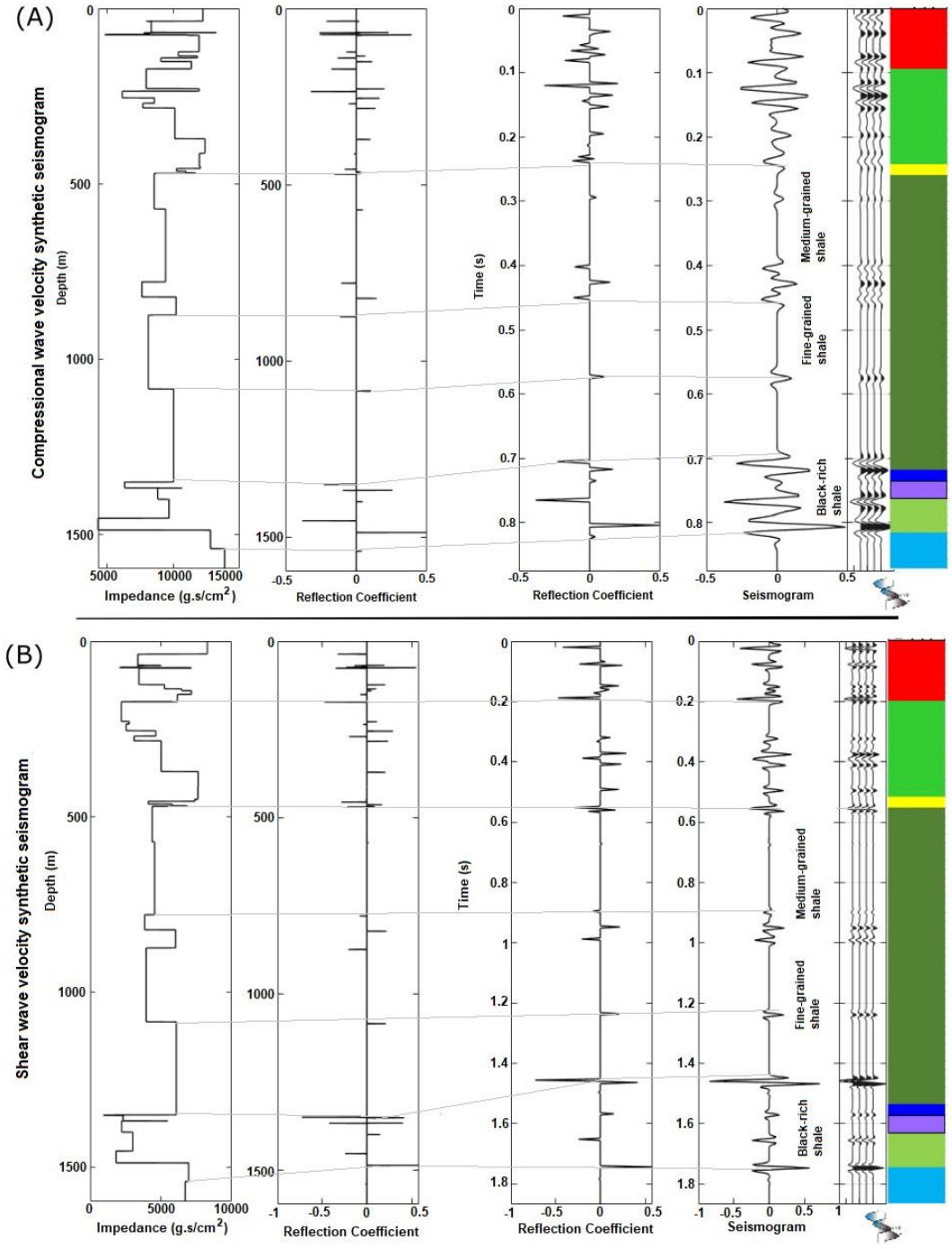


Figure 5-2: Synthetic seismogram of P-wave (a) and S-wave (b) generated using 40 Hz frequency against the stratigraphy associated with borehole lithology.

5.7 Legacy seismic reflection data acquisition and processing

The seismic data were acquired in the 1960s by Soeker (Southern Oil Exploration Corporation) in the southern part of the Karoo Basin (Figure 5.3 a, b). The seismic survey was designed to explore for hydrocarbons in the Karoo Basin. A Geophex dynamite source with an average weigh of 20 kg was used in holes (~ averaging 17 m in depth) (Fatti and du Toit, 1970) with geophone spacing of 50 m. Table 5.10 shows the acquisition parameters for the seismic survey.

Table 5-10: Table for acquisition parameters of reconnaissance seismic- reflection traverses including WK06_01 and WK06_02 survey lines.

Survey acquisition parameters	
Acquisition mode	Conventional split-spread
Geophone	14 Hz
Geophone group	24
Geophone number	12 (set-up along the profile line)
Group spread distance	50 m
Geophone group separation	50 m
Survey spread length	1200 m
Amplifiers	Geospace mode SSCIII
Instrument	Techno-type analogue (amplitude modulated)
Acquisition filter	Band-pass filter (22 – 108 Hz) Cut-off slopes 36DV/ Octave
Play back filter	20-60 Hz
Shot points	Single holes 15 m – 18 m deep using failing rotary drill
Group wavelength	11/12λ

Data were corrected for a low velocity layer 2130 m/s at surface. The seismic data were processed using a standard procedure, including static corrections, NMO, CDP stacking, band-pass filtering (Fatti and du Toit, 1970). A velocity of 4546 m/s was used for elevation correction. The dominant frequency of the data is 40 Hz (Fatti and du Toit, 1970).

The laboratory P-wave velocity measurements of the shale core samples range from 1715 m/s to 4561 m/s. The calculated P-wave velocity range (V_a) and dominant frequency (F_D) resulted in the dominant wavelength ($\lambda=V_a/F_D$) range of 43 m and 114 m. Therefore, using the quarter wavelength criteria, the minimum resolvable thickness of the shale layer could range

from 11 m to 28 m (i.e., vertical resolution limit) (Widess, 1973). For the migrated data, the horizontal resolution ranges from 43 m to 114 m.

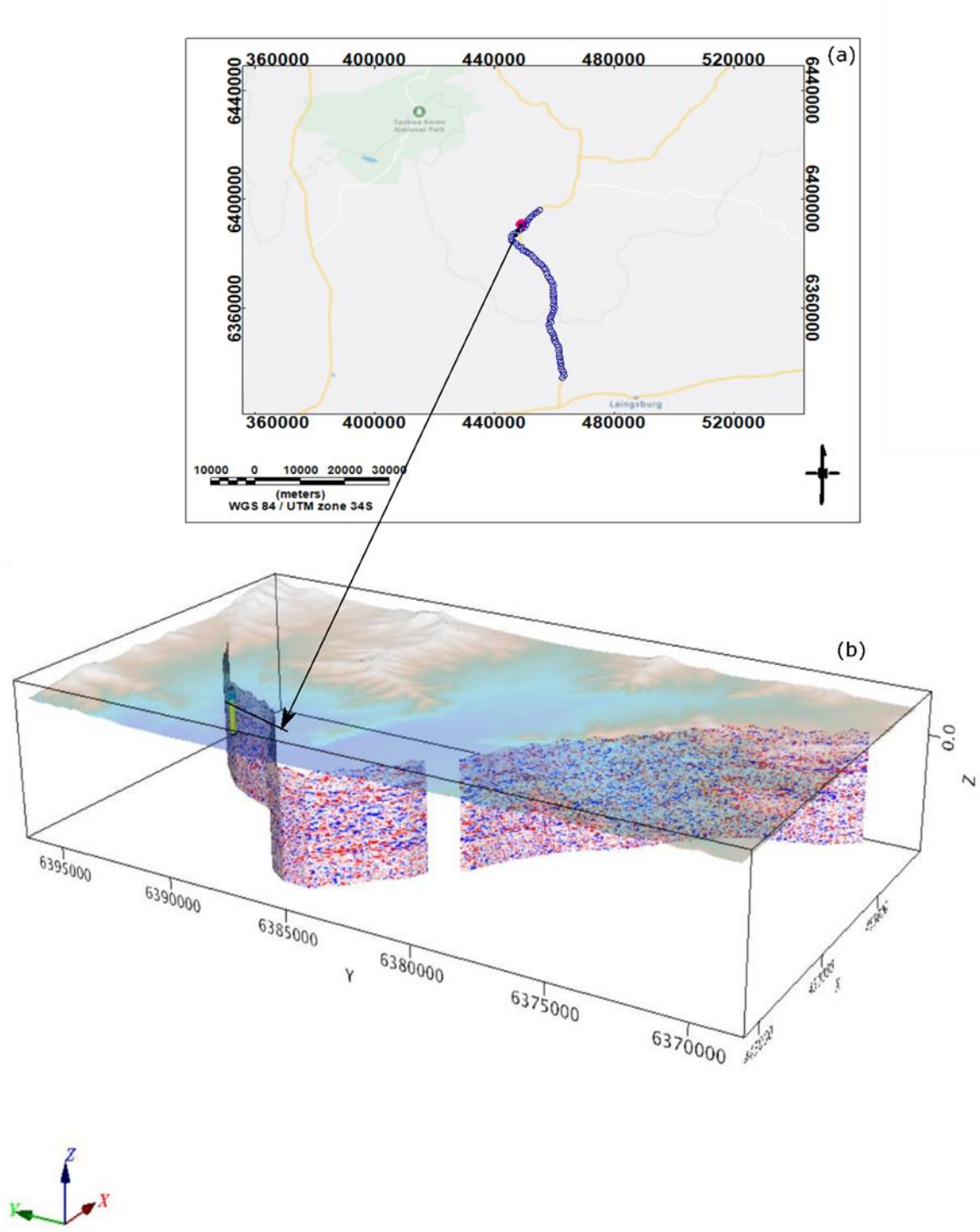


Figure 5-3: (a) Location of the seismic profile WK06_01 and WK06_02 and borehole KL1-65 (pink circle) on Google map (b) Imported location map from oasis Montaj in relation to the position of KL1-65 borehole (yellow) and seismic sections WK06_01 and WK06_02.

5.8 XRD and petrography results

Thin sections of five samples are shown from Figure 5.4 to 5.8. Table 5.11 summarises the results from XRD. The rocks from the Waterford Formation, uppermost formation of the Ecca Group, are dominated by both microcrystalline and polycrystalline quartz, feldspar (i.e. albite) and micas (Figures 5.4 and 5.5). Similarly, the argillaceous and arenaceous rocks of the lower Ecca Group (Whitehill and Collingham Formations) are dominated by both microcrystalline and polycrystalline quartz, feldspar (i.e., albite) and micas. These rocks are exhibit a crystalline texture set in a fine-grained matrix of muscovite, sericite, clay minerals (kaolinite, smectite, illite), feldspar, and quartz (Figures 5.6 -5.8).

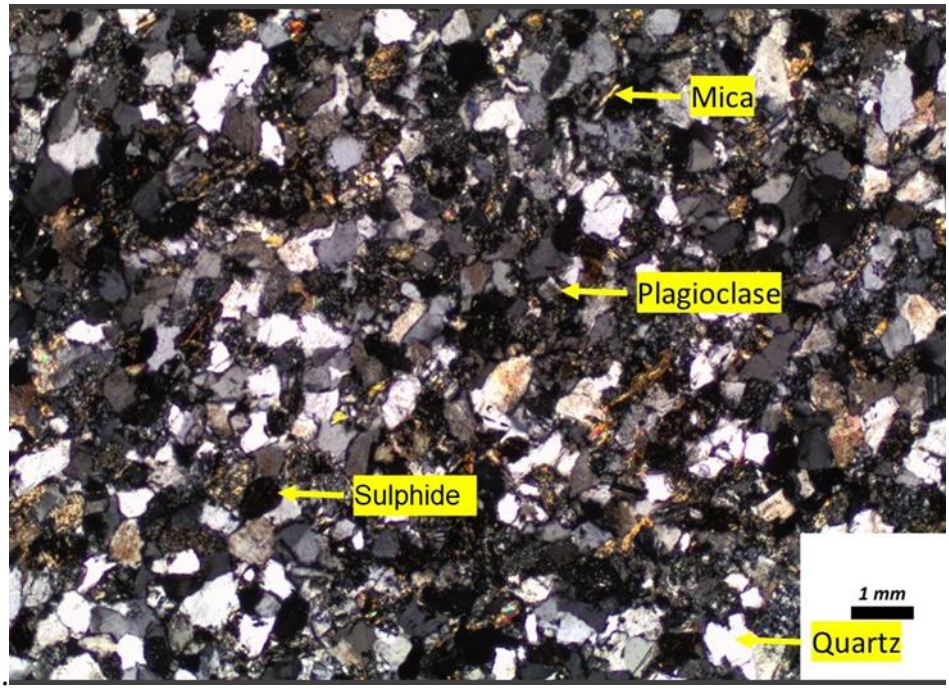


Figure 5-4: Thin section petrography of SM05 showing composition dominated by quartz, followed by plagioclase and alteration of plagioclase, then mica and other clay minerals.

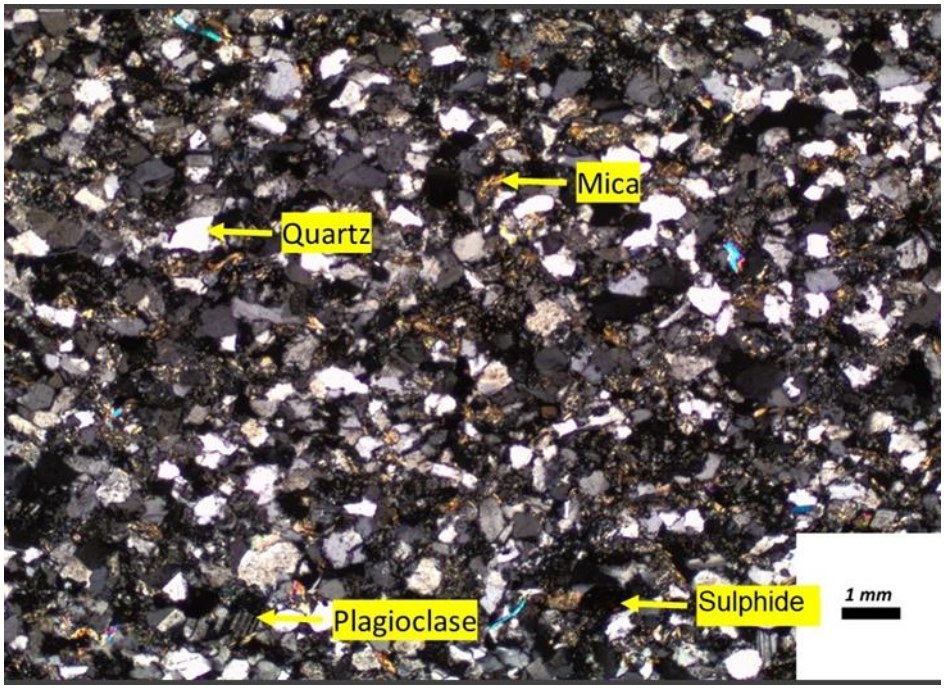


Figure 5-5: Thin section petrography of SM12 showing composition dominated by quartz, followed by plagioclase and its alteration as well as mica and other clay minerals.

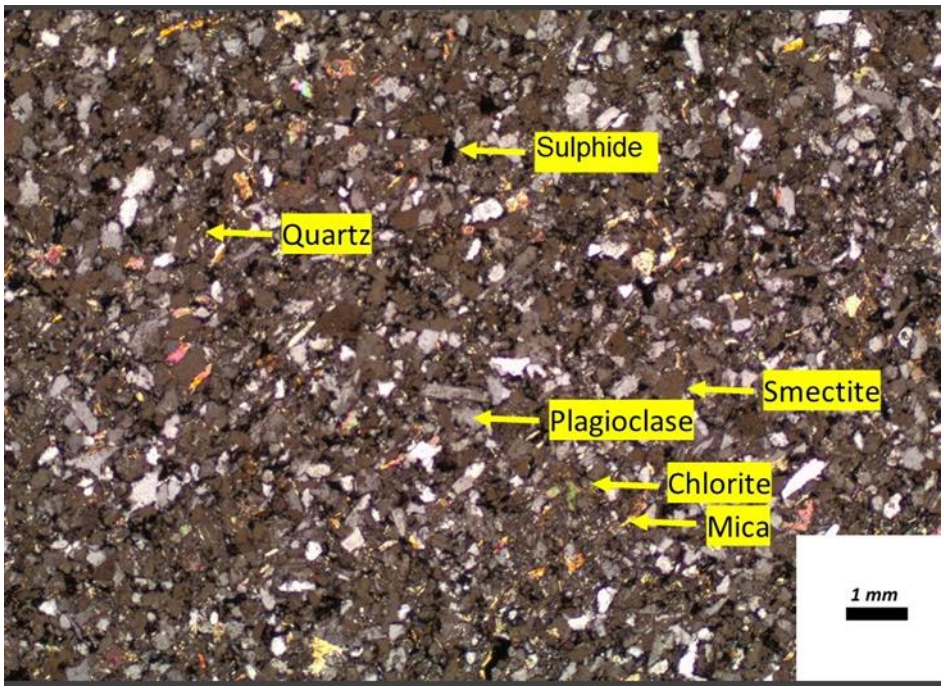


Figure 5-6: Thin section petrography of SM30 showing dominant composition of quartz followed closely by plagioclase and handful of smectite as well as other clay-rich mineral including mica.

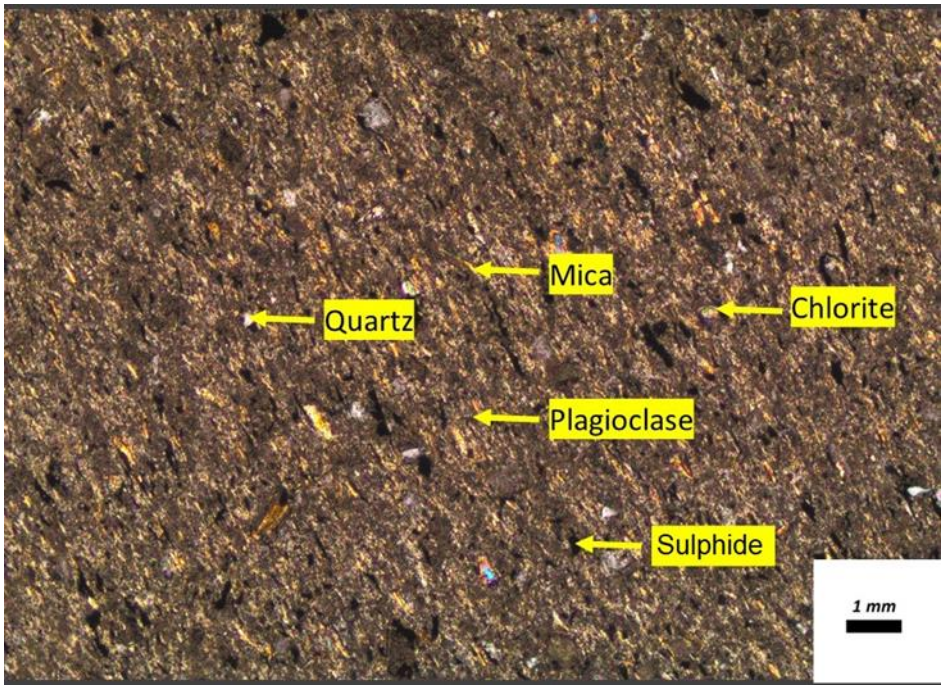


Figure 5-7: Thin section petrography of SM42 showing dominant composition of quartz followed closely by mica with other clay-rich mineral and handful of smectite as well as plagioclase.

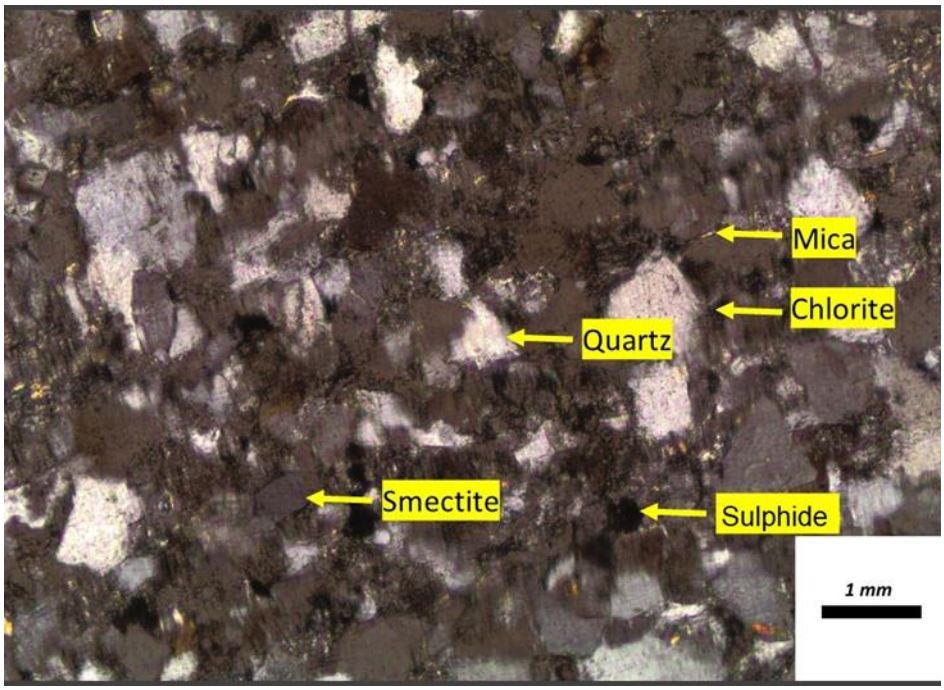


Figure 5-8: Thin section petrography of SM39 showing dominant composition of quartz followed closely by mica with other clay-rich mineral and handful of smectite as well as plagioclase.

Table 5-11 : XRD results of five samples, two sandstone, one siltstone and two samples.

Sample ID	Quartz	Calcite	Plagioclase	Mica	Chlorite	Smectite	Sulphides	clay-rich	Lithology
SM05	62	1	31	4		2			Sandstone
SM12	57	1	33	5	2	1	1		Sandstone
SM30	51	1	38	7	1	1	1		Siltstone
SM39	45		4	29	1	5	2	10	Shale
SM42	49		4	29	1	5	2	10	Shale

.

6 INTERPRETATION AND DISCUSSION

In this study an investigation on different methods that can be used to measure density and velocity measurements was undertaken. Mineral composition of five representative rock samples was determined using thin section and XRD. Velocity measurements under pressure (or stress) were investigated on five samples.

6.1 Density vs velocity

Most studies have demonstrated that the seismic velocities tend to increase with density, and these observations are supported by the famous Nafe-Drake relationship (e.g., Nkosi *et al*, 2017). However, in this study which is looking specifically at the sedimentary rocks from the Karoo, shows no direct linear relationship between seismic velocities and densities for most lithologies except for the Dwyka samples whose samples are limited to two. The shale samples showed a lot more indication of no linear relationship between seismic velocity and density the most as compared to other lithologies (Figure 6.1). This may indicate that mineralogy, fractures, grain size, temperature, porosity, and depth may have major effects on the seismic velocities. However, these effects cannot be easily tested with laboratory experiments.

Seismic reflectivity is controlled mostly by acoustic impedance between lithological contacts (Salisbury *et al*, 2003). The bulk density and velocity measurements of each sample were used to calculate the acoustic impedance and reflection coefficients. The density values of shale samples show an overall decrease with depth from 2.630 g/cm^3 in the Waterford Formation to 2.114 g/cm^3 when reaching the more carbonaceous zones (Lower Ecca Group). Similarly, the P-wave velocities of shale show a decrease with depth from 4696 m/s in Waterford Formation to 2592 m/s in the Whitehill Formation. The Whitehill Formation shale

tends to have lower impedances than the shale in the Upper Ecca Formation. Therefore, the contrast in acoustic impedances between the upper and lower Ecca Group is significant enough to result in high amplitude reflections and identify the interface with the more carbonaceous shale layer. For example, the interface between shale layers is presented by SM30 and SM31 (Table 5.9).

On average, the density measurements of sandstones exhibit higher densities compared to the rest of sedimentary rocks within the Karoo Basin. For example, SM01 has a density of 2.620 g/cm^3, which is relatively higher than most samples (mainly siltstones and some shales) in this study. The sandstone samples also exhibit relatively high velocity values (e.g., Vp ~ 5500 m/s for SM05). Therefore, significant contrast in acoustic impedances between sandstones and other sedimentary rocks are expected, e.g., between the interface of siltstone sample (SM11) and sandstone (SM12) (Table 5.9).The densities obtained from siltstone are a mixture of the shale and sandstone density values, and this may explain a wide variation in siltstone values observed on the P-wave velocity versus density graph (Figure 6.1).

The Dwyka tillite has very high velocity values (Table 5.7). Additionally, they exhibit high density values as compared to the Prince Albert shale layer overlying it. Therefore, the difference in acoustic impedance between the two layers will be significant and result in high reflections 0.51 as observed on Table 5.9.

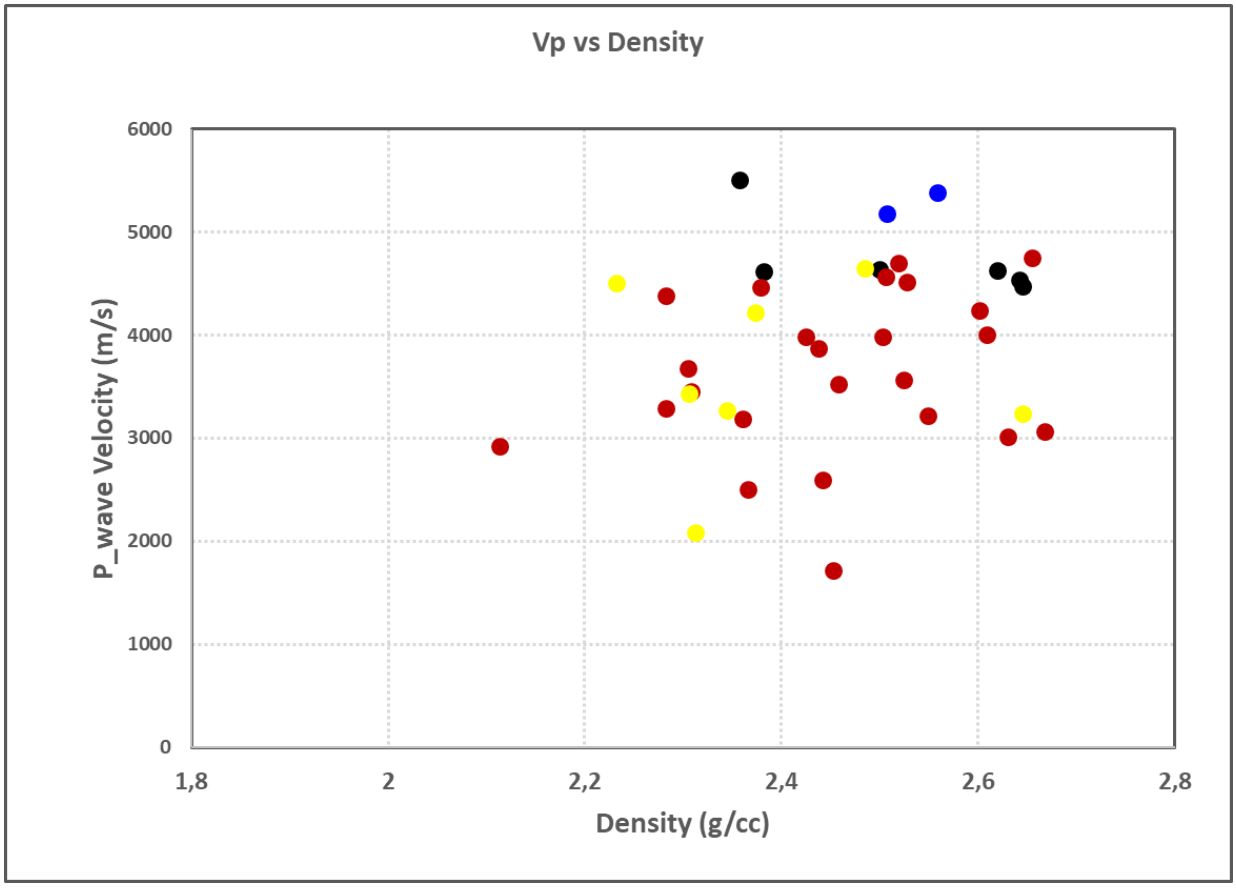


Figure 6-1: P-wave velocity measurements of all samples plotted against density with red dots representing the shale sample, yellow representing the siltstone, black representing the sandstone and the blue representing the Dwyka tillites.

6.2 Relationship between Vp and Vs

Obtaining a rock sample is by far the surest way to determine the lithology and rock type. However, measurements of velocity are another way of indirectly identifying the different lithologies. The ratio of P-wave velocity to S-wave velocity is an important parameter to identify lithology (Mokhtar, 2012). Figure 6.2 shows the relationship between Vp and Vs for all samples measured. The ratio between Vp and Vs for sandstone samples was found to be approximately less than 1.60, which indicates that the rock materials are unconsolidated (Lee, 2003) (Figure 6.2a). Agreeably so, most sandstone samples were obtained in shallow depth area and were prone to weathering. Therefore, the equation

$$y = 0.074x + 4500 \quad (15)$$

where y is Vp and x is Vs, could be used to estimate the velocity of sandstone in the shallow depth (150 m) of the Karoo Basin in areas where rock samples are not available.

Furthermore, the equation can also be used for lithological identification of shallow depth sandstone units in the Karoo Basin.

The Vp against Vs values of all the siltstone samples are also plotted in Figure 6.2b. By using the graph, the following equation was obtained:

$$y = 1.523x + 400 \quad (16)$$

where y is Vp and x and Vs.

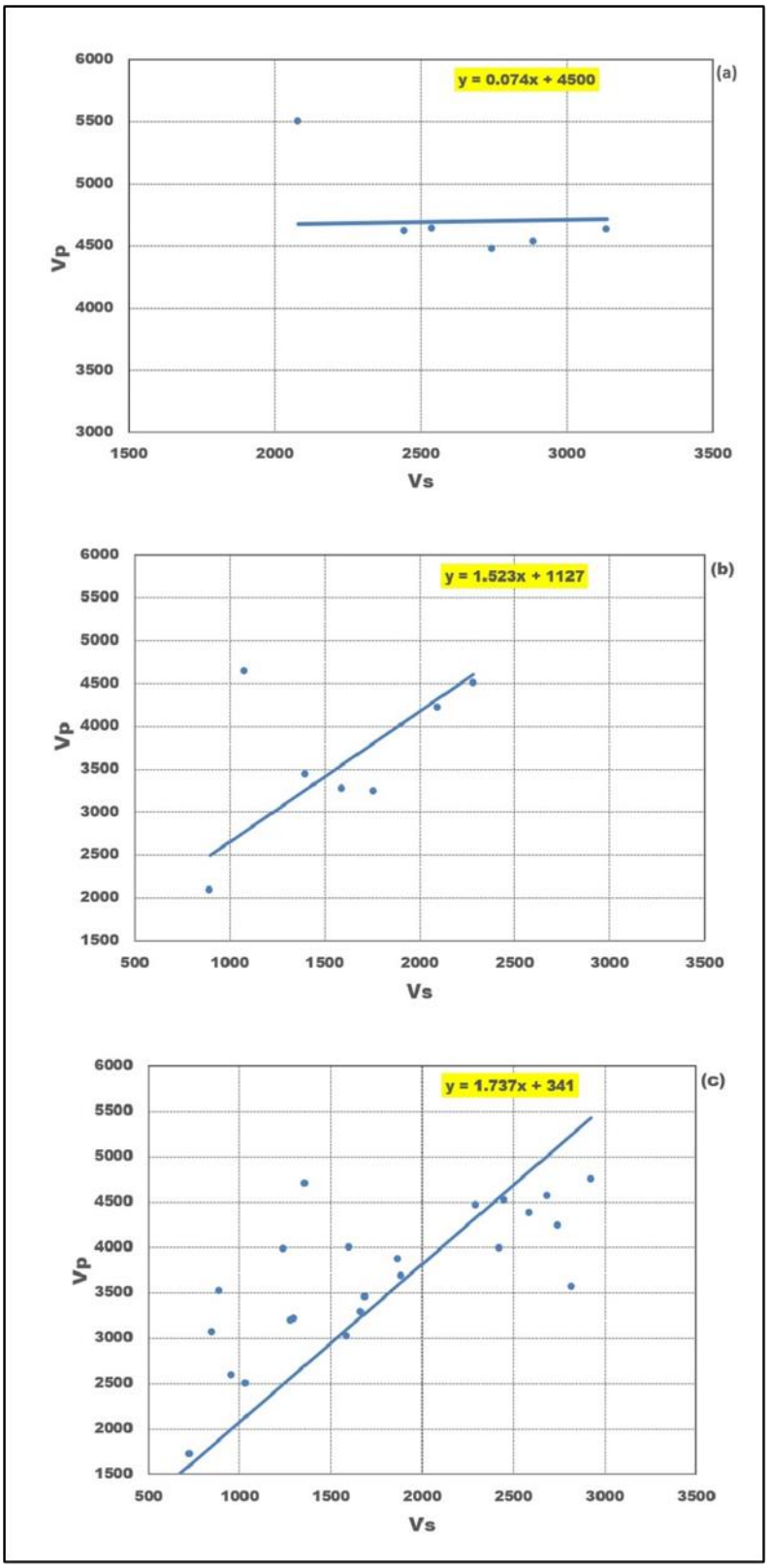
However, these values are found to be higher than values obtained using Castagna *et al.* (1985)'s equation of:

$$Vs = 0.862Vp - 1.172 \quad (17)$$

The Vp against Vs values of all shale samples are plotted in Figure 6.3c, and the average ratio was calculated by line of best fit to be 1.73. According to Greenberg and Castagna (1992) this value suggests that most of shale samples are organic-rich. The equation of:

$$y = 1.737x + 341 \quad (18)$$

where y is Vp and x is Vs, could be used for identification of organic-rich shale formation.



(b)

(c)

Figure 6-2: Vp vs Vs plots for sandstone (a), siltstone (b), and shale (c) obtained from borehole KL1-65 showing equation obtained for each lithology using the best line fit.

In general velocities are observed to be increasing with depth (Figure 6.3**)**. Large variations of Vp/Vs ratio are observed at shallow depth implying that the lithology at the top of the borehole may be unconsolidated suggesting large Poisson ratio values to be expected. Agreeably so, large values of Poisson ratio (ν) are observed in the top 300 m of the borehole (Figure 6.4). In general, the rest of the borehole is observed to be between 0.2 and 0.5 which is slightly higher than a bracket of rock material ranging $0.1 \leq \nu \leq 0.4$ (Logo and Vasarhelyi 2019). Otherwise, most of the borehole samples were observed to be intact. No additional data were obtained from downhole logs to confirm any geological structure in place.

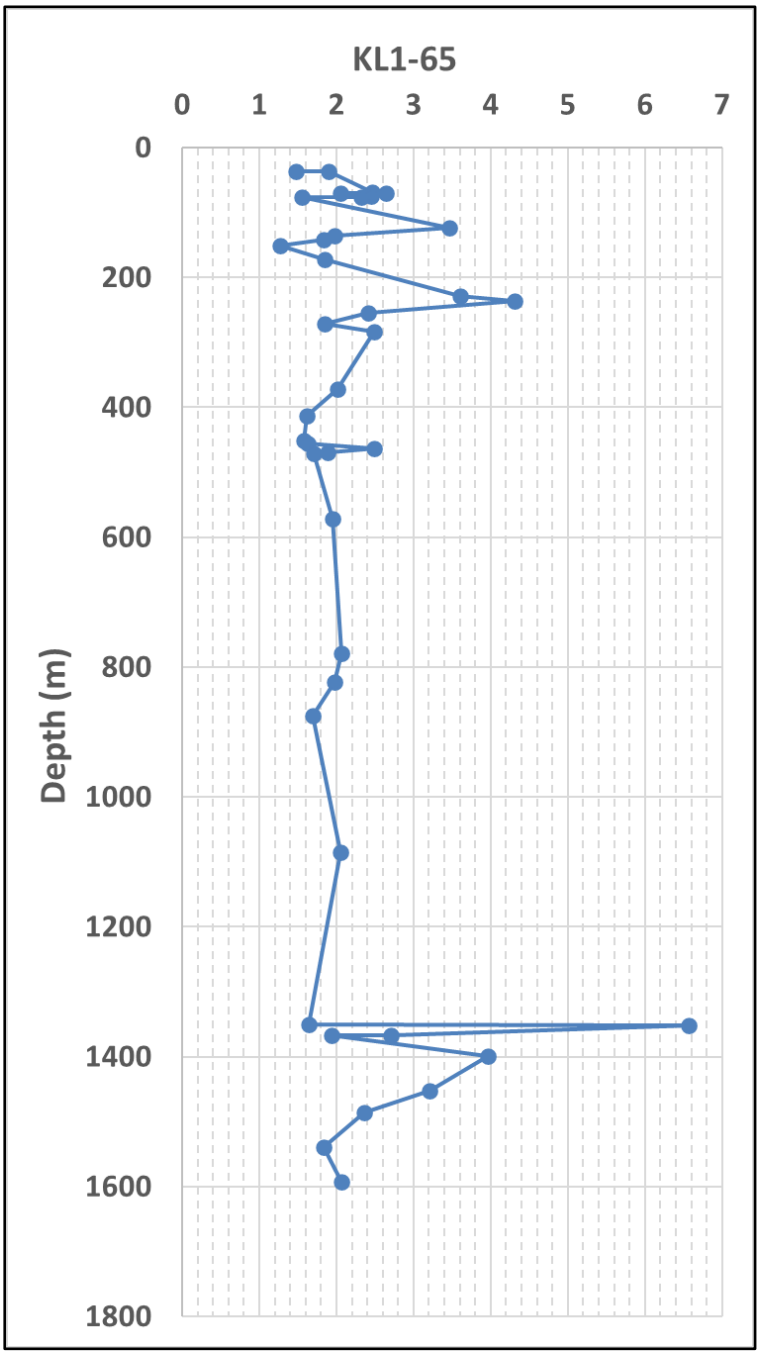


Figure 6-3*:* Relationship between Vp/Vs with regards to depth.

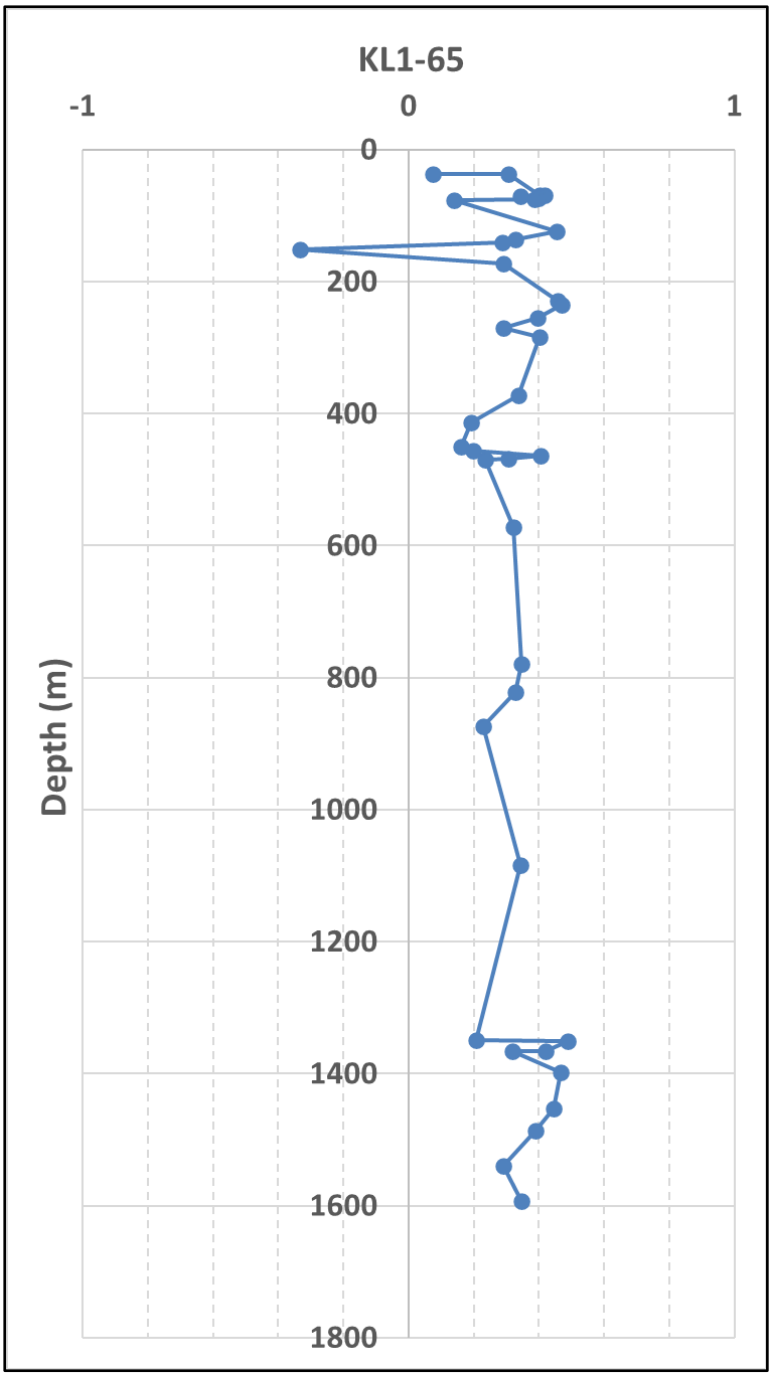


Figure 6-4: Poisson ratio against depth for borehole KL1-65.

6.3 Effect of minerals on seismic velocity

Petrological analysis was conducted on five samples at the Council for Geoscience Mineralogy laboratory to determine the effect mineralogy and grain-size has on seismic velocities. The sandstone packages comprise mainly quartz, which generally exhibits relatively high seismic velocity values (Li and Gu, 2015) as compared to most minerals within the sedimentary rocks. Higher composition of quartz ensures higher possibility of quartz-to-quartz

contact which improves transmission of acoustic waves throughout the sample. SM05 and SM12 are representatives of the sandstone packages and comprise different minerals. SM05 is a medium-grained sandstone with 62% quartz and SM12 is fine-grained with 57% quartz. SM05 has 5% more quartz as SM12, as expected, SM05 exhibits higher velocity (5500 m/s) than SM12 (4640 m/s).

Shale packages are mostly clayey which may slow down transmission of acoustic waves resulting in relatively lower seismic velocity values. SM42, for example, is a fine-grained shale with dominating quartz (49%) composition followed by mica with other clay-rich mineral (39%), smectite (5%), plagioclase (4%), sulphide (2%) and chlorite (1%). SM39 is similar to SM42 in mineral composition except it contains less quartz. However, SM30 is medium-grained shale and comprises mainly quartz (51%), followed by plagioclase (38%), mica (7%), and others (4%). The high percentage of quartz presents in SM30 might have attributed to high P-wave velocity of 4561 m/s. This difference in quartz composition between the three samples may explain major differences in P-wave velocities obtained between SM (Vp~4561 m/s and Vs~2684 m/s), SM39 (Vp~2592 m/s and Vs~956 m/s) and SM42 (Vp~3980 m/s and Vs~1240 m/s).

6.4 Effect of stress on seismic velocities

Nkosi et al. (2017) shows that the seismic wave velocities can be controlled by the stress applied to the sample. The reason for this is that the sample under-stress tends to have high rigidity which is caused by a closure of micro-fractures and grain contacts.

In this study, the P-wave velocities of five samples were measured under constant increasing uniaxial stress in order to investigate the effect of stress on seismic velocities. Generally, samples with higher quartz content cannot sustain higher pressure and reach their saturation stage at lower elevated pressure. The P-wave velocities measured under stress varied considerably (see Figure 5.6).

For example, SM05 with 62% of quartz reached P-velocity saturation at 45 MPa, while SM12 with 57% of quartz reached P-wave velocity saturation stage at 60 MPa. Additionally, the shale samples are observed to be able to sustain more pressure before reaching saturation stage. The two shale sample, SM42 and SM40, reached P-velocity saturation at elevated pressure of 60 MPa and 80 MPa, respectively. The shale samples have higher clay mineral content (39%), which may indicate high porosity (Alansari, 2019). The increase in P-wave

velocity with pressure is associated with the closure of pores and micro-fractures during compaction as pressure is elevated. For example, shale withstands pressure by first closing in on all the fracture and pores within the rock before reaching saturation stage. The gradual increase in P-wave velocity in shale is due to the closure of pores and fractures. Unlike the shale samples, the sandstone sample has low porosity, hence there is no major effect of stress on seismic velocities. For example, the grain-to-grain interaction happens so rapidly forcing the sample to reach saturation stage at an earlier elevated pressure. The sharp increase at an early loading stage on the sandstone samples are probably due to rapid closure of pores and fractures.

It is, however, worth noting that there were no clear fractures that were observed in the samples. Further studies could be done to determine the presence of small fractures in the samples, and also to determine their origin (i.e., natural fractures or drilling induced fractures).

6.5 Synthetic seismogram and seismic interpretation

The synthetic seismogram presented in Figure 6.4 shows strong reflections packages (RP1-RP4). The RP1 at TWT of 0 - 0.3 s indicates the interface between Waterford-Kookfontein, Kookfontein-Skoorsteenberg and Skoorsteenberg-Tierberg Formation with interbedded shale deposit. The reflection is due to the significant acoustic impedance contrast between the sandstone and siltstones with velocities ranging between 2080 and 5500 m/s and a density range of 2.30 – 2.69 g/cm^3. The RP2 and RP3 at TWT of 0.45 and 0.58 s, respectively, represent the intercalated carbonaceous shale within the Tierberg Formation. Additionally, the RP4 at TWT of approximately 0.7 – 0.79 s represents interfaces between Tierberg, Collingham, Whitehill and Prince Albert Formation, while RP5 at TWT of approximately 0.82 s is the Dwyka Group-Prince Albert Formation boundary.

To investigate the source of reflections observed on the legacy reflection seismic data, 1D synthetic seismograms (Figure 6.5) were correlated with the seismic section (Figure 6.6a). The results show that reflections (RP2-RP4) observed on seismograms correspond to those observed in the seismic section (Figure 6.6b) while RP1 in the top section of the seismic section was not resolved. The reflections RP5 is observed on the seismic section at approximately TWT 1.3 s. The depth for RP5 was estimated to be approximately 2.4 km using average velocity values of shale obtained from Bokkeveld (RSA PPD) of 3736 m/s. This strong reflector maps the bottom of the Dwyka Group and top pf the Bokkeveld Group. The seismic

sections also show additional deeper reflections, RP6 and RP7, (Figure 6.6c) representing Bokkeveld Boundary (BV) and Table Mountain Basement boundary (TBM) as per Fatti, 1970's interpretation. RP6 and RP7 are at 2.0 s and 2.9 s, respectively. The RP5, RP6 and RP7 reflections do not appear on the synthetic seismograms as the borehole was only sampled to 1600 m (Figure 6.5).

Following of the correlation of the seismic data with 1D synthetic models, structural interpretation was done on a seismic section. The seismic section exhibits two normal half-graben faults (F1 and F2) dipping in the opposite direction **(**Figure 6.6c**)**. These faults cross-cut and displace the TBM, but do not displace base of the TBM. Similarly, F3, F4 and F5 were also observed on Figure 6.7a and picked on Figure 6.7b. F3 and F4 form horst and graben structures within the Lower Ecca Group dipping in different direction. F4 is observed to cross-cut the Upper Ecca, Lower Ecca and Bokkeveld Group while F3 cuts across only the Ecca Group. These faults may represent post-rift deformational structures. Moreover, F5 is a normal syn-rift depositional fault dipping towards the southwest. The undulating characteristic of the basement surface is also observed.

Summarily, integrated Geoscience data (geology, physical properties measurements, synthetic seismogram, and seismic sections) were used to create a geological model in Figures 6.6b and 6.7b, and reduce the interpretational ambiguity associated with geophysical dataset. Thus, the Upper Ecca, Lower Ecca including the Dwyka, Bokkeveld Group, Table Mountain Group and Basement Natal interfaces, and fault structures were successfully delineated. Additionally, the synthetic seismograms revealed the several reflectors within the Tierberg Formation. The first reflector (RP2) is associated change in grain size where medium-grained shale at the top of the lithological group becomes fine-grained. The second reflector (RP3) is associated with the fine-grained shale becoming more carbonaceous. The last reflector (RP4) is associated with fine-grained carbonaceous shale becoming black-rich shale with increase in pyrite, (Chere 2005) within the Tierberg Formation (Figures 6.5 and 6.6). All the reflectors correlated well with the reflections seismic signatures seen on the seismic sections.

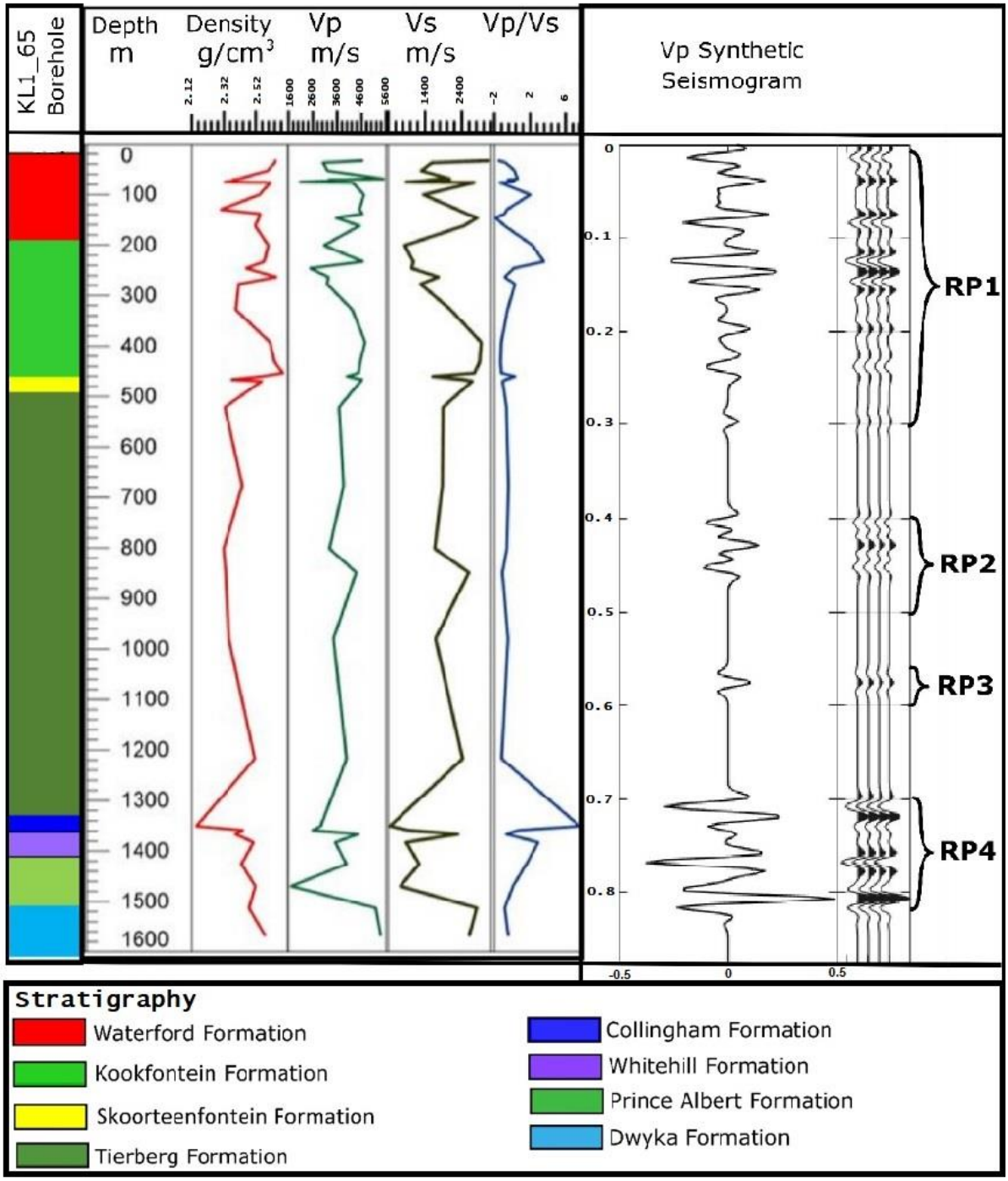


Figure 6-5: Synthetic seismogram generated using 40 Hz Ricker wavelet, together with velocity and density laboratory measurements. Note, the RP1 indicates interface between Waterford-Kookfontein, Kookfontein-Skoorsteenberg, and Skoorsteenberg-Tierberg Formation with interbedded shale deposit; the RP2 and RP3 represent the change in grain size within the shale in the Tierberg Formation; and the RP4 represents intercalated black-rich rich from the Tierberg Formation onwards.

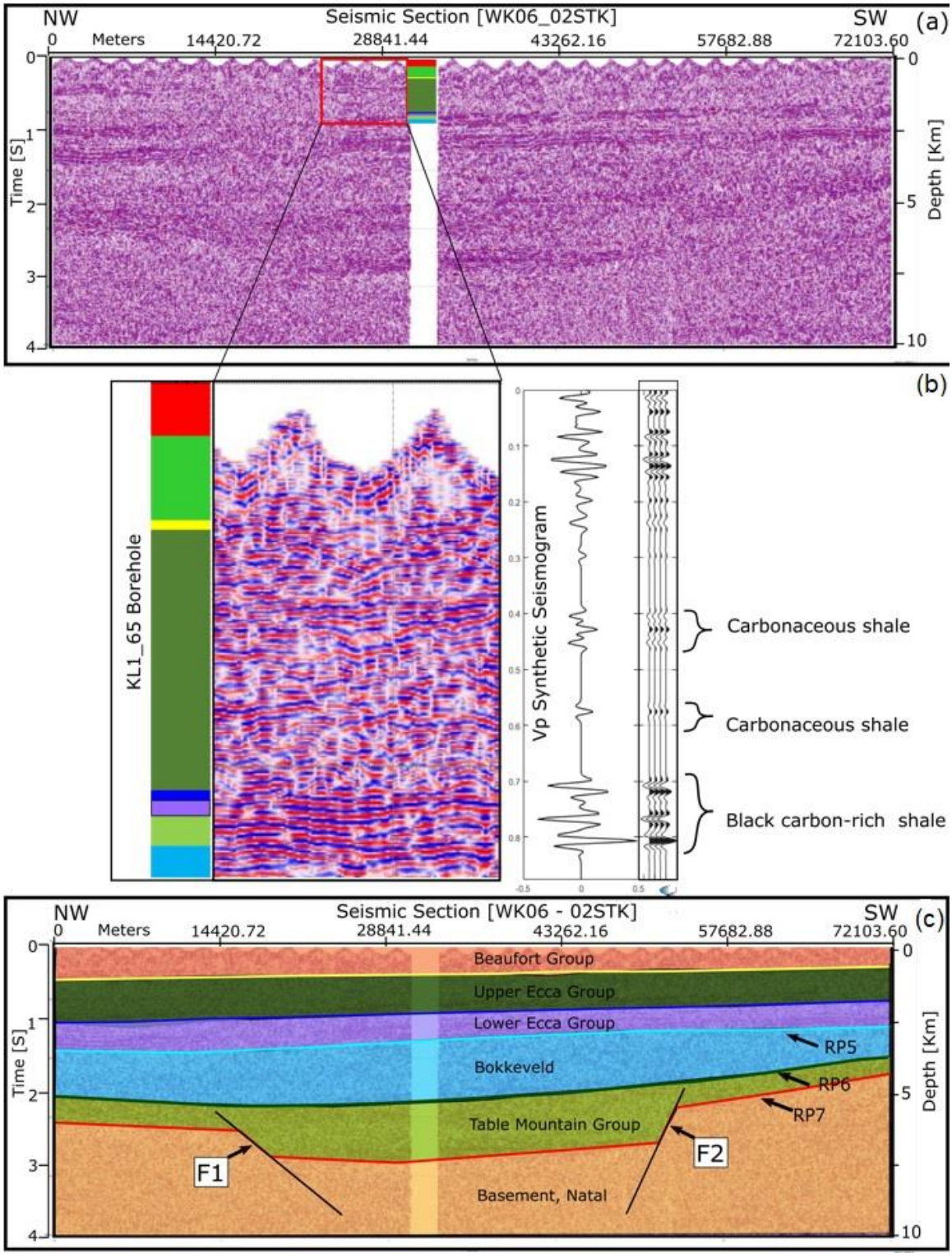


Figure 6-6: (a) Time -migrated seismic section WK06_02, the red block indicates the extracted seismic part to correlate with the KL1-65 borehole, (b) the KL1-65 borehole correlated with the seismic section and the synthetic seismogram (c) interpreted seismic section indicating the Beaufort Group, Upper Ecca, Lower Ecca, Dwyka and Table Mountain Group. Note, average layered velocity of 5000 m/s was used to estimate the depth values; the black lines represent the faults.

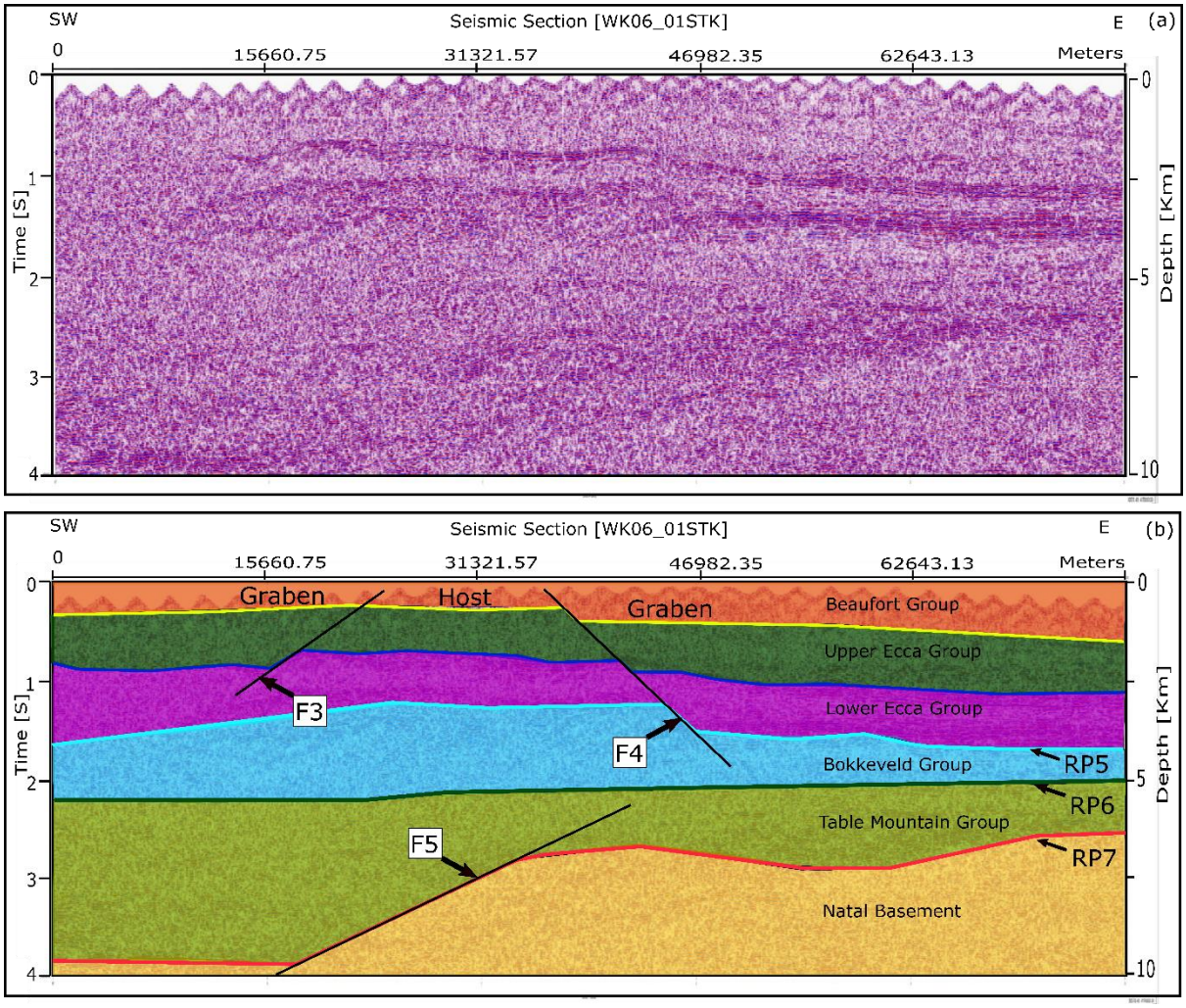


Figure 6-7: (a) Time -migrated seismic section WK06_01, (b) Interpreted seismic section WKO6_01 indicating the Upper Ecca, Lower Ecca, Dwyka and Table Mountain Group. The black lines represent the faults delineated on the seismic line; average layered velocity of 5000 m/s was used to estimate the depth values.

7 CONCLUSION AND RECOMMENDATION

Laboratory measurements of bulk density and seismic velocity were carried out in this study. The effect of stress and mineralogy on seismic velocities were also investigated. Three different methods were used to estimate the bulk density values in order to obtain the accurate and most representative measurement for each lithology, as well as to reduce experimental errors. Among the three experimental methods, water displacement with coated wax method was found to be more accurate compared to the rest of the methods. This method was useful for most samples including the fractured and porous rock types. However, to conduct more accurate measurements, fresh core samples would be preferable.

Laboratory measurements of seismic velocities on rock samples were undertaken using two different instruments, namely the Tektronix and Proceq system. The experimental setup plays a paramount role in the credibility of the results. Tektronix system was suitable for seismic velocity measurements under uniaxial stress when compared to the Proceq system. Linear relationship between Vp and Vs was observed, and the generated equations could be used for lithology identification of sandstones and shale in the Karoo Basin for future studies. To improve the equations' reliability, additional fresh core samples should be acquired to yield better representative results. When plotting densities against velocity, no linear relationship was observed for most samples. Furthermore, it was observed that the mineral composition has an impact on the seismic wave velocities, thus it is important to incorporate mineralogy information in future seismic studies. For example, it was observed that two sandstone samples with different mineral composition produce different seismic velocities. The fine-grained samples with lesser quartz content resulted in lower velocity values as compared to medium-grained sample with high quartz content samples.

To understand the effect of pressure, seismic velocities were measured under uniaxial stress. The results indicated that velocity increases as function of stress and reaches a constant phase where all the pores and fractures are completely closed in a sample. The results suggested that stress, in addition to mineralogy and density, should be incorporated in future seismic studies in the area. However, it is recommended that future studies should consider ultrasonic measurements under confined stress to mimic the *in-situ* environment.

In addition, the legacy reflection seismic sections revealed several reflectors that indicated boundaries between stratigraphical units and fault structures. The generated synthetic seismogram models successfully revealed the contact between the shale and carbonaceous

shale within the Lower Ecca Group, which showed good correlation with reflections observed on the seismic section. Finally, the integration of all geoscientific datasets played a major role in generating a geological model of the study area as well as reducing the ambiguities in the geophysical data interpretation.

8 REFERENCES

Alansari, A., Salim, A., Janjuhah, H., Bin Abd Rahman, A., and Fello, N. (2019). Quantification of clay mineral microporosity and its application to water saturation and effective porosity estimation: A case study from Upper Ordovician reservoir, Libya. Journal of Natural Ga Seoscience, 4(3), 139-150.

Anderson, N.L., Hedke, D E., and Knapp, R W. (1995). Forward seismic modelling-Applications and utility. Kansas Geological Survey.

Berryman, J.G. (2007). Seismic waves in rocks with fluids and fractures. Geophysical Journal International,171, 954-974.

Black, B.E. (2015). Stratigraphic characterisation of the Collingham Formation in the context of shale gas from a borehole (SFT 2) near Jansenville, Eastern Cape, South Africa. Volume 153 of Bulletin (Council for Geoscience).

Boadu, F.K., Long, L.T. (1996). Effects of fractures on seismic-wave velocity and attenuation. Geophysical Journal International, 127, 86-110.

Cadle, A.B, Cairncross, B., Christiec, A.D.M., and Roberts, D.L. (1993). The Karoo Basin of South Africa: type basin for the coal-bearing deposits of southern Africa. International Journal of Geology, 23, 117-157.

Castagna, J., Batzle, M.L., Eastwood, R.L. (1985). Relationship between compressional and shear-wave velocities in classic silicate rocks. Geophysics, 50, 571-581.

Catuneanu, O., Wopfner, H., Eriksson, P.G., Cairncross, B., Rubidge, B.S., Smith R.M.H., and Hancox, P.J. (2005). The Karoo basins of south-central Africa, Journal of African Earth Sciences, 43, 211-253.

Chen, H., Jiang, B., Chen, T., Xu, S., Zhu, G. (2017). Experimental study on ultrasonic velocity and anisotropy of tectonically deformed coal. International Journal of Coal Geology, 179, 242-252.

Chere, N. (2015). Sedimentological and geochemical investigations on borehole cores of the Lower Ecca Group black shales, for their gas potential - Karoo Basin, South Africa. MSc Thesis, Nelson Mandela Metropolitan University.

Christensen, I., and Wang, F. (1985). The influence of pore pressure and confining pressure on dynamic elastic properties of Berea sandstone. Society of Exploration Geophysics, 50, 207-213.

Coetzee, J. (2018). Integration of seismic attributes and physical property measurements to study hydrocarbon reservoirs, offshore Orange Basin and Main Karoo Basin, South Africa. MSc Thesis, University of the Witwatersrand, Johannesburg.

Cole, D.I. and Wipplinger, P.E. (2001). Sedimentology and molybdenum potential of the Beaufort Group in the Main Karoo Basin. Memoir, Council for Geoscience, South Africa, 80, 225.

Cole, D.I., Robey, K, Chevallier, L. and Viljoen, J. (2011). Report on the geology of shales with a gas potential in the Main Karoo Basin of South Africa. Unpublished Report of the Council for Geoscience, Western Cape Regional Office, 2011-0142.

Crawford, K.M. (2013). Determination of bulk density of rock core using standard industry methods. Master Thesis, Michigan Technological University.

De V. Wickens, H., and Cole D.I. (2017). Lithostratigraphy of the Kookfontein Formation (Ecca Group, Karoo Supergroup), South Africa. South African Journal of Geology, 120 (3), 447-458.

Ding, P., Di, B., Wang, D., Wei, J., and Li, X. (2014). P And S wave anisotropy in fractured media: Experimental research using synthetic samples. Journal of Applied Geophysics, 109, 1-6.

Fatti, J.J.L. and du Toit J.L. (1970). A regional reflection-seismic line in the Karroo Basin near Beaufort West. South African Journal of Geology, 73 (1), 17-27.

Fener, M. (2011). The Effect of Rock Sample Dimension on the P-Wave Velocity. Journal Non-destructive Evaluation, 30:99–105DOI 10.1007/s10921-011-0095-7.

Geel C., De Wit M., Booth P., Schultz H.M., and Horsfield B. (2015). Shale Gas characteristics of Permian black shales, Ecca group, Eastern Cape, South Africa. South African Journal of Geology, 118(3), 249-274.

Greenberg, M. L., Castagna, J. P. (1992). Shear-wave velocity estimation in porous rocks: theoretical formulation, preliminary verification and applications. Geophysical Prospecting,40(2), 195-209.

Halliday, D. and Resnick, R. (1988). Fundamentals of Physics, 3rd ed.

Handwerger, D.A., Cooper, A.K., O'Brien, P.E., Williams, T., Barr, S.R., Dunbar, R.B., Leventer, A., and Jarrard, R.D. (2004). Synthetic seismograms linking ODP sites to seismic profiles, continental rise and shelf of Prydz Bay, Antarctica. In Cooper, A.K., O'Brien, P.E., and Richter, C. (Eds.), Proceedings of the Ocean Drilling Program, Scientific Results, 188, 1-28.

Johnson, M.R., Anhaeusser, C.R., and Thomas, R.J. (2006). The Geology of South Africa. ISBN: 9781919908779.

Karaman, K., Kaya, A., and Kesimal, A. (2015). Effect of the specimen length on ultrasonic P-wave velocity in some volcanic rocks and limestones. Journal of African Earth Science, 112, 142-149.

Kearey, P., Brooks, M., and Hill I. (2002). An Introduction to Geophysical Exploration: John Wiley and Sons, 3, 21-98.

Krebes, E.S. (2004). Seismic forward modelling. CSEG Recorder.

Kuuskraa, V. and Moodhe, K., (2013). Technically recoverable shale gas and shale oil resources: An assessment of 137 shale formations in 41 countries outside United State. Prepared for : U.S. Energy information Administration and U.S. Department of Energy.

Lee, M.W (2003). Velocity Ratio and its Application to Predicting Velocities. U.S. Geological Survey Bulletin, p 2197.

Li, Y., and Gu, H. (2015). The relationship between mineral content and acoustic velocity of sandstone reservoirs in Junggar basin. Journal of Geophysics and Engineering (12), 629-637.

Liu, L., Li, L., Elsworth, D., Zhi, S., Yu, Y., (2018). The impact of oriented perforations on fracture propagation and complexity in hydraulic fracturing. Processes, 6(11), 213.

Lerwill, W. E. (1979). Developments in Geophysical Exploration Methods, 115-14.

Logo, B.A. and Vasarhelyi, B. (2019). Estimation of the Poisson's rate of the intact rock in the function of the rigidity. Periodica Polytechnica Civil Engineering, 63(4), 1030 - 1037.

Manzi, M.S.D., Durrheim R.J., Hein K.A.A. and King N. (2012). 3D edge detection seismic attributes used to map potential conduits for water and methane in deep gold mines in the Witwatersrand basin, South Africa. Geophysics, 77, WC133-WC147.

Malumbazo, N. (2016). Report on MTEF shale gas: deep borehole and geo-environmental. Unpublished Report of the Council for Geoscience, Pretoria Head Office, 2016-0082.

Mokhtar, E.A., Vega S, Hassan, A.A, Baloushi, MA. (2012). Porosity and heterogeneity effect on Vp/Vs ratio in carbonate rocks from a reservoir in the Middle East, poster presentation, AAPG international conference and exhibition, Milan, Italy.

Nkosi, N.Z., Manzi, M.S.D., Drennan, G. and Yilmaz, H. (2017). Experimental measurements of seismic velocities on core samples and their dependence on mineralogy and stress; Witwatersrand Basin (South Africa). Studia Geophysica et Geodaetica, 61, 115-144.

Redpath, B.B. (1973). Seismic refraction exploration for engineering site investigations. Geology.

Rubidge, B.S. (2005). Re-uniting lost continents - Fossil reptiles from the ancient Karoo and their wanderlust. South African Journal of Geology, 108, 135-172.

Salisbury, M.H., Harvey, C.W., and Matthews, L. (2003). The acoustic Properties of Ores and Host rocks in Hardrock Terranes. Hardrock Seismic Exploration, 9-19.

Schmitt, D.R. (2015). Geophysical Properties of the Near Surface Earth: Seismic Properties. Treatise on Geophysics, 11,43-87

Sheriff, R.E. (1984). Encyclopedic dictionary of Exploration Geophysics, Society of Exploration Geophysicists, Tulsa Oklahoma, 69-70

Sheriff, R.E. and Geldart, L.P. (1995). Exploration Seismology, 2nd Cambridge University Press.

Spagnolia, G., Weymer, A.B., Jegen, M., Spangenberg, E., and Petersen, S. (2017). P-wave velocity measurements for preliminary assessments of the mineralization in seafloor massive sulfide mini-cores during drilling operations. Engineering Geology, 226, 316-325.

Stein, S., and Wysession, M. (2003). An Introduction to Seismology, Earthquakes, and Earth Structure, Blackwell Publishing, Malden, Massachusetts, USA., 134-157

Telford W.M., Geldart L.P., and Sheriff R.E. (1990). Applied Geophysics 2nd ed, 136-232.

Visser J.N.J. (1985). The Dwyka Formation along the north-western margin of the Karoo Basin in the Cape Province, South Africa. South African Journal of Geology, 88 (1).

Visser J.N.J. (1992). Deposition of the Early to Late Permian Whitehill Formation during aa sea-level high stand in a juvenile foreland basin. South African Journal of Geology, 95, 181-193

Von Brunn V. (1996). The Dwyka Group in the northern part of Kwazulu/Natal, South Africa: sedimentation during late Palaeozoic deglaciation. Palaeogeography, Palaeoclimatology, Palaeoecology,125 (1-4), 141-163

Westgate, M., Manzi, M.S.D. James, I., and Harrison, W. (2020). New insights from legacy seismic data: reprocessing of legacy 2D seismic data for imaging of iron-oxide mineralisation near Sishen Mine, South Africa. Geophysical Prospecting, 68, 1-22.

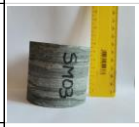
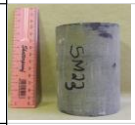
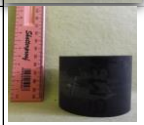
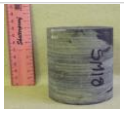
Widess, M.B. (1973). How thin is a thin bed? Geophysics, 38, 1176-1180.

Yilmaz, O. (2001). Seismic data analysis - Processing, inversion, and interpretation of seismic data, Tulsa: Society of Exploration Geophysicists.

Zhang, R., Jiang, B., and Cao, W. (2002). Influence of sample size on ultrasonic phase velocity measurements in piezoelectric ceramics. Journal of Applied Physics, 91.

Appendix A

List of samples and measurements of samples saved on a disk.

Sample ID	Lithology		Sample ID	Lithology		Sample ID	Lithology		Sample ID	Lithology		Sample ID	Lithology	
SM01	Sandstone		SM10	Shale		SM19	Siltstone		SM30	Shale		SM39A	Shale	
SM02	Shale		SM11	Siltstone		SM21	Shale		SM31	Shale		SM40	Shale	
SM03	Shale		SM12	Sandstone		SM22	Siltstone		SM32	Shale		SM41	Shale	
SM05	Sandstone		SM13	Shale		SM23	Shale		SM33	Shale		SM42	Shale	
SM06	Siltstone		SM15	Shale		SM25	Sandstone		SM34	Shale		SM43	Shale	
SM07	Siltstone		SM16	Shale		SM26	Sandstone		SM35	Shale		SM44	Tillite	
SM08	Siltstone/Shale		SM17	Siltstone		SM28	Shale		SM36	Shale		SM45	Tillite	
SM09	Shale		SM18	Shale		SM29	Sandstone		SM37	Shale				

Appendix B

Density values summarised from RSA PPD.

Sandstone	Density (g/cm^3)		
Formation	min	max	mean
Clarens	2.390	2.62	2.55
Molteno	2.451	2.52	2.454
Burgesdorp	2.379	2.804	2.509
Tarkastad	2.375	2.479	2.447
Balfour	2.573	2.657	2.588
Abrahamskraal	2.374	2.68	2.612
Adelaide	2.382	2.75	2.66
Fort Brown	2.612	2.653	2.637
Ripon	2.362	2.675	2.611
Collingham	2.589	2.643	2.625
Vryheid	2.570	2.59	2.589
Ecca	2.140	3.04	2.643

Shale	Density (g/cm^3)		
Formation	min	max	mean
Waterford	2.122	2.709	2.404
Burgesdorp	2.310	2.75	2.58
Tarkastad	2.570	2.677	2.616
Balfour	2.644	2.659	2.647
Abrahamskraal	2.590	2.759	2.606
Upper Ecca	2.528	2.53	2.529
Volksrust	2.110	3.62	2.5
Vryheid	1.674	2.554	2.23
Lower Ecca	1.600	2.55	2.15
Whitehill	2.513	2.747	2.616
Prince Albert	2.210	2.86	2.47

P-wave velocity values summarised from RSA PPD

Shale	P-wave velocity (m/s)		
Formation	min	max	mean
Adelaide	2660	5350	4450
Upper Ecca	3545	5121	4606
Volkrust	2432	5588	4202
Tierberg	2514	4903	3624
Vryheid	774	4475	2350
Whitehill	3329	5675	4605
Pietermaritzburg	2952	3676	3496
Prince Albert	3786	5170	4659
Lower Ecca	1290	5250	3220

Sandstone	P-wave velocity (m/s)		
Formation	min	max	mean
Clarens	1341	2211	1523
Vryheid	980	5500	3454

Siltstone	P-wave velocity (m/s)		
Formation	min	max	mean
Vryheid	1710	2474	1899

Tillites	P-wave velocity (m/s)		
Formation	min	max	mean
Dwyka	4500	5500	5210